A mechanism for controlled breakage of under-replicated chromosomes during mitosis

Duda, Heike ; Arter, Meret ; Gloggnitzer, Jiradet ; Teloni, Federico ; Wild, Philipp ; Blanco, Miguel G ; Altmeyer, Matthias ; Matos, Joao

Abstract: While DNA replication and mitosis occur in a sequential manner, precisely how cells maintain their temporal separation and order remains elusive. Here, we unveil a double-negative feedback loop between replication intermediates and an M-phase-specific structure-selective endonuclease, MUS81-SLX4, which renders DNA replication and mitosis mutually exclusive. MUS81 nuclease is constitutively active throughout the cell cycle but requires association with SLX4 for efficient substrate targeting. To preclude toxic processing of replicating chromosomes, WEE1 kinase restrains CDK1 and PLK1-mediated MUS81-SLX4 assembly during S phase. Accordingly, WEE1 inhibition triggers widespread nucleolytic breakage of replication intermediates, halting DNA replication and leading to chromosome pulverization. Unexpectedly, premature entry into mitosis—licensed by unrestrained CDK1 activity during S phase—requires MUS81-SLX4, which inhibits DNA replication. This suggests that ongoing replication assists WEE1 in delaying entry into M phase and, indirectly, in preventing MUS81-SLX4 assembly. Conversely, MUS81-SLX4 activation during mitosis promotes targeted resolution of persistent replication intermediates, which safeguards chromosome segregation.

DOI: https://doi.org/10.1016/j.devcel.2016.11.017

A mechanism for controlled breakage of under-replicated chromosomes during mitosis

Heike Duda[1], Meret Arter[1,4], Jiradet Gloggnitzer[1,4], Federico Teloni[2,4], Philipp Wild[1], Miguel G. Blanco[3], Matthias Altmeyer[2] and Joao Matos[1,5]

[1]Institute of Biochemistry, HPM - ETH Zürich, Otto-Stern-Weg 3, 8093 Zürich, Switzerland.
[2]Department of Molecular Mechanisms of Disease, University of Zurich, Winterthurerstrasse 190, 8057 Zürich, Switzerland.
[3]Departamento de Bioquímica e Bioloxía Molecular, CIMUS, Universidade de Santiago de Compostela, Avda. de Barcelona, 15706 Santiago de Compostela, Spain.

[4]These authors contributed equally to this work
[5]Corresponding author: tel +(41) 44 63 36115
e-mail: joao.matos@bc.biol.ethz.ch

Key words: Cell-cycle, WEE1, CDK1, PLK1, DNA replication, MUS81, SLX4, chromosome pulverization

Running title: MUS81-EME2-SLX4 pulverizes under-replicated chromosomes during mitosis

SUMMARY

While DNA replication and mitosis occur in a sequential manner, precisely how cells maintain their temporal separation and order remains elusive. Here, we unveil a double-negative feedback loop between replication intermediates and an M-phase-specific structure-selective endonuclease, MUS81-SLX4, which renders DNA replication and mitosis mutually exclusive. MUS81 nuclease is constitutively active throughout the cell cycle, but requires association with SLX4 for efficient substrate targeting. To preclude toxic processing of replicating chromosomes, WEE1 kinase restrains CDK1 and PLK1-mediated MUS81-SLX4 assembly during S-phase. Accordingly, WEE1 inhibition triggers widespread nucleolytic breakage of replication intermediates, halting DNA replication and leading to chromosome pulverization. Unexpectedly, premature entry into mitosis -licensed by unrestrained CDK1 activity during S-phase- requires MUS81-SLX4, which inhibits DNA replication. This suggests that ongoing replication assists WEE1 in delaying entry into M-phase and, indirectly, in preventing MUS81-SLX4 assembly. Conversely, MUS81-SLX4 activation during mitosis promotes targeted resolution of persistent replication intermediates, which safeguards chromosome segregation.

INTRODUCTION

Stable propagation of the genome entails replication of genetic material and segregation of duplicated sets of chromosomes prior to cell division. In eukaryotic cells these events are separated in time, with gap phases often inserted between the two (S-phase and M-phase). It was long assumed that replication intermediates act as negative regulators of mitotic entry in order to prevent the catastrophic segregation of partly replicated DNAs (Enoch and Nurse, 1991; Hartwell and Weinert, 1989). Recent work has challenged this view and it is increasingly well established that even unperturbed cells sometimes enter mitosis with under-replicated chromosomes, especially if replication stalls late during S-phase (Mankouri et al., 2013). How cells adjust M-phase initiation to the completion of DNA replication and how replication intermediates are resolved when mitotic entry precedes the conclusion of DNA synthesis remains poorly understood.

Timely and orderly rounds of DNA replication and segregation require oscillatory phosphorylation events carried out by cyclin-dependent kinases (CDKs). While S- and M-phase cyclin-CDK complexes display a varying degree of functional overlap, it is crucial for cells to suppress M-phase CDK levels during DNA replication. In agreement, Xenopus egg extracts supplemented with high amounts of cyclin B initiate DNA synthesis, but soon after halt S-phase and enter mitosis prematurely (Moore et al., 2003). Likewise, in fission yeast and human cells in culture, a surge in CDK activity leads to mitotic entry despite the presence of incompletely replicated chromosomes (Coudreuse and Nurse, 2010; Heald et al., 1993; Jin et al., 1998). Alongside numerous other studies, these observations show that manipulation of the overall CDK activity levels is sufficient to change the order of cell cycle events.

To establish the appropriate length of S-phase, cells adjust the levels of CDK activity through inhibitory phosphorylation. The conserved WEE1 and MYT1 kinases mediate this phosphorylation event, whereas phosphatases of the CDC25 family promote the reverse reaction (Pines, 1999). This mode of CDK regulation is vital for genome integrity, especially when problems arise during DNA replication. The ATR kinase responds to stalled DNA replication by activating CHK1, a checkpoint kinase that interfaces with CDC25 and WEE1, to inhibit CDK1 and delay the onset of mitosis (Jackson and Bartek, 2009; Zhou and Elledge, 2000). Interestingly, besides

licensing premature entry into mitosis, down-regulation of WEE1 or CHK1 causes CDK-dependent breakage of replicating chromosomes (Beck et al., 2010; Beck et al., 2012; Dominguez-Kelly et al., 2011; Forment et al., 2011). In turn, CDC25A over-expression leads to replication fork (RF) reversal, which is also followed by CDK1-dependent DNA cleavage (Neelsen et al., 2013).

The mechanism by which WEE1/CDC25/CHK1 misregulation causes chromosome breakage is not fully understood. Yet, several studies established that it involves MUS81, a structure-selective endonuclease with important roles in the metabolism of replication intermediates (Beck et al., 2012; Dominguez-Kelly et al., 2011; Forment et al., 2011; Kim et al., 2013; Neelsen et al., 2013; Techer et al., 2016). In mammals, MUS81 forms heterodimeric complexes with the non-catalytic subunits EME1 or EME2 (Pepe and West, 2014a). Both MUS81-EME1 and MUS81-EME2 are capable of cleaving Y-shaped duplex DNAs in vitro, suggesting that RFs may be physiological MUS81 substrates in vivo (Pepe and West, 2014b). In agreement with this notion, MUS81 has been implicated in the nucleolytic processing of stalled RFs after prolonged S-phase arrest (Hanada et al., 2007). Moreover, by cleaving persistent replication intermediates during M-phase, MUS81 promotes DNA repair synthesis outside S-phase and safeguards faithful chromosome segregation (Minocherhomji et al., 2015; Naim et al., 2013; Ying et al., 2013).

It remains elusive, though, how cells achieve efficient processing of stalled RFs after prolonged arrest or in M-phase, while avoiding the toxic cleavage of related DNA structures during unperturbed S-phase. Since WEE1 kinase prevents MUS81-dependent DNA breakage, it has been suggested that WEE1 may directly phosphorylate and inhibit MUS81, specifically during S-phase (Dominguez-Kelly et al., 2011). On the other hand, MUS81-mediated processing of Holliday junctions (HJs), generated during recombinational DNA repair, is upregulated at the onset of mitosis (Gallo-Fernandez et al., 2012; Matos et al., 2011; Matos et al., 2013; Szakal and Branzei, 2013; Wyatt et al., 2013). CDK1-dependent interaction with the scaffold protein SLX4 coordinates the nickase activity of another structure-selective nuclease, SLX1, with subsequent HJ incision by MUS81 (Castor et al., 2013; Fekairi et al., 2009; Gritenaite et al., 2014; Matos et al., 2011; Munoz et al., 2009; Svendsen et al., 2009; Wyatt et al., 2013). Hence, regulated activation of MUS81 at the G2/M transition could provide an alternative explanation for its limited ability to cleave RFs

during S-phase, while efficiently processing stalled replication intermediates at the onset of mitosis.

Here, we have investigated how cells dynamically adjust MUS81 nuclease activity towards replication intermediates during the cell cycle. Unexpectedly, by outlining the mechanism of MUS81 control, we reveal its pivotal role within a regulatory network that ensures that DNA replication and mitosis occur sequentially and in a mutually exclusive manner. MUS81 regulation avoids detrimental cleavage of replication intermediates, which can lead to chromosome pulverization.

RESULTS

MUS81 nuclease is constitutively active throughout the cell cycle

To investigate if MUS81 activity towards replication intermediates is regulated during the cell cycle we immunopurified MUS81-FLAP, expressed at endogenous levels, from cells collected at 2-hr intervals after release from a double-thymidine block. We then incubated the immunoprecipitated (IP) material with a synthetic Y-shaped dsDNA structure that resembles branched DNA at the RF, and is a bona fide substrate of recombinant MUS81 (Pepe and West, 2014b). Incubation of this model RF with MUS81-FLAP IPs resulted in robust cleavage of the substrate (Figure 1A-C). Notably, however, MUS81 activity remained unchanged throughout the time course (Figure 1A-C). To confirm this result, we compared the activity of MUS81 from cells synchronized at G1/S with cells synchronized in prometaphase. MUS81 IPs from both cell cycle stages showed similar kinetics in RF processing (Figure S1A-C).

Since cleavage of Holliday junctions (HJs) by MUS81 is cell cycle regulated and increases upon SLX1-SLX4 binding at the G2/M transition (Figure S1D, left panel) (Castor et al., 2013; Matos et al., 2011; Wyatt et al., 2013), we tested whether SLX1 also stimulates MUS81 activity on model RF substrates. In contrast to HJ processing, depletion of SLX1 did not noticeably reduce the ability of MUS81 IPs to process model RFs (Figure 1D and Figure S1E). This does not exclude the possibility that the function of a fraction of MUS81 nuclease may be modulated by protein-protein interactions and/or post-translation modifications. However, these data suggest that the catalytic activity of MUS81 is neither inhibited prior to mitosis, nor globally stimulated through interaction with SLX1-SLX4 nuclease.

SLX4 controls the association of multiple MUS81 molecules and their recruitment to under-replicated regions during mitosis

MUS81 is known to associate with chromatin at under-replicated regions during mitosis (Naim et al., 2013; Ying et al., 2013). Since MUS81-SLX4 association occurred with similar timing, we examined if SLX4 also binds chromatin in mitosis and whether it plays a role in MUS81 recruitment. To follow SLX4 localization, we

used immunofluorescence microscopy in cell lines stably expressing SLX4-FLAP. In cells with condensed chromatin, indicative of mitotic entry, SLX4-FLAP was frequently enriched in discrete foci, whose number varied between cells (Figure 1F). The majority of mitotic SLX4-FLAP co-localized with MUS81 and with known components of stalled replisomes (Figure 1E, data not shown)(Gritenaite et al., 2014; Naim et al., 2013; Pedersen et al., 2015; Ying et al., 2013).

We next asked whether SLX4 is required for targeting MUS81 to stalled replication intermediates. In agreement with recent reports (Guervilly et al., 2015; Minocherhomji et al., 2015), we found that SLX4 depletion strongly impaired MUS81 recruitment to subnuclear foci during mitosis (Figure 1G and H). Accordingly, SLX4 depletion caused a 10-fold decrease in MUS81 recruitment to TOPBP1 foci (Figure 1I).

Besides targeting MUS81 to stalled replication intermediates during mitosis, we noticed that SLX4 regulates MUS81 through an additional mechanism. Analysis of MUS81-FLAP IPs showed that endogenous MUS81 was enriched in nocodazole- but not in thymidine-treated cells (Figure S1A, Figure S2A, data not shown). Since MUS81-SLX4 interaction occurred with a similar timing (Figure S2A), we asked whether association of multiple MUS81 molecules might be SLX4-dependent. Indeed, upon depletion of SLX4, endogenous MUS81 was no longer detected in MUS81-FLAP IPs (Figure S2B). Therefore, SLX4 promotes association of multiple MUS81 molecules, specifically at the onset of mitosis.

Phosphorylation of SLX4 is required for MUS81 binding during mitosis

In previous work, we showed that MUS81-SLX4 association requires CDK1 activity, but its direct substrate(s) in this process remain elusive (Wyatt et al., 2013). Since SLX4 is phosphorylated at 30 of 41 minimal CDK consensus sites (S/TP) (Figure 2A), we sought to generate an SLX4 mutant fully refractory to CDK-phosphorylation. To this end we engineered *SLX4*^{41A}, which encodes alanine substitutions of all serines or threonines preceding a proline. Expression of FLAG-tagged SLX4^{41A} in HeLa cells revealed that the alanine substitutions did not impair SLX4 stability, compared to SLX4^{WT} (Figure 2B). In addition, SLX4^{41A} IPs showed

normal association with both SLX1 and XPF, indicating that the folding of the mutant protein was largely preserved. Notably, however, $SLX4^{41A}$ IPs lacked MUS81 (Figure 2B), suggesting that phosphorylation may promote a domain-specific change in SLX4 required for MUS81 binding. Since MUS81 interacts with the SAP domain of SLX4 (Figure 2A)(Castor et al., 2013; Kim et al., 2013), we mutated the 6 S/TP sites on the C-terminus of SLX4, and generated $SLX4^{6A}$. In addition, we generated the complementary mutant by targeting the remaining 35 sites ($SLX4^{35A}$). Remarkably, while $SLX4^{35A}$ showed normal binding to MUS81, mutation of the 6 S/TP sites surrounding the SAP domain abolished SLX4-MUS81 complex formation (Figure 2C). These data argue that CDK1-mediated phosphorylation of the SAP domain in SLX4 is part of the M-phase-specific switch that controls MUS81 association.

WEE1 inhibits CDK1 to prevent MUS81-SLX4 association during S-phase

Our results led us to suspect that, rather than inhibiting MUS81 activity directly, as previously suggested (Dominguez-Kelly et al., 2011), WEE1 suppresses toxic processing of replication intermediates by preventing MUS81-SLX4 association during S-phase. To test this hypothesis we synchronized cells at G1/S, and released cultures in the presence of the small molecule inhibitor MK-1775 (hereinafter referred to as WEE1i), which has been extensively validated for selective inhibition of WEE1 in vitro and in vivo (Aarts et al., 2012; Beck et al., 2012; Hirai et al., 2009). We then immunoprecipitated SLX4 from samples collected at 2-hr intervals and analyzed the immunoprecipitated material for the presence of MUS81. Whereas control cells showed MUS81-SLX4 association 6 hrs after release from thymidine, cells treated with WEE1i showed similar levels of MUS81-SLX4 interaction already 2 hrs after release (Figure 2D).

Since the SLX4-MUS81 complex forms at the G2/M transition, we examined if changes in SLX4-associated RF-processing activities were detected throughout the cell cycle. Indeed, SLX4-FLAP IPs showed a strong increase in RF cleavage shortly before mitotic entry, which correlated with MUS81 association (Figure 2D and E, left panels). Importantly, siRNA-mediated depletion of MUS81 reduced the prometaphase-specific increase in RF-processing activity of SLX4 IPs (Figure S2C).

Moreover, inhibition of WEE1 advanced the peak of SLX4-associated RF processing in time, further strengthening a model in which WEE1 prevents SLX4 complexes from acquiring the ability to process replication intermediates prematurely (Figure 2D and E). In contrast, the RF-processing activity of MUS81 IPs remained constant, confirming that WEE1 does not directly inhibit the nuclease activity of MUS81 (Figure S2D). Under identical experimental conditions, MUS81-mediated HJ processing increased upon SLX4-SLX1 association and, accordingly, was advanced in time as a consequence of WEE1 inhibition (Figure S1D).

Since WEE1 phosphorylates CDK1 to reduce its activity during S-phase (Russell and Nurse, 1987), we reasoned that WEE1 could indirectly restrain MUS81-SLX4 interaction. To test this scenario we inhibited CDK1 (RO-3306) or PLK1 (BI2536) in cells treated with WEE1i and analyzed MUS81-SLX4 complex formation. Inhibition of CDK1 reduced MUS81-SLX4 association during S-phase and strongly reduced the ability of SLX4 IPs to process model RFs (Figure 2D and E). Upon PLK1 inhibition, we observed a delay of ~6 hrs in MUS81-SLX4 association, which was mirrored by late activation of SLX4 to process model RFs (Figure 2D and E). WEE1 inhibition also induced a CDK1-dependent electrophoretic mobility shift in SLX4, during S-phase (2-6 hr after thymidine release) (Figure 2D). This is consistent with a model in which CDK1-mediated phosphorylation of SLX4 directly controls MUS81 association (Wyatt et al., 2013)(Figure 2D).

WEE1 activity prevents recruitment of MUS81-SLX4 nuclease to replicating chromosomes during S-phase

We next examined if binding to SLX4 elicited recruitment of MUS81 to replicating chromosomes. We released pre-synchronized cells to undergo S-phase in the presence or absence of WEE1 inhibitor, and imaged MUS81 and SLX4 at different time points after release (3 hrs and 9 hrs, to enrich for S-phase and mitosis, respectively). 98% of all S-phase cells treated with WEE1i showed widespread MUS81 and SLX4-FLAP chromatin association and extensive colocalization (Figure 2F). The majority of control cells (93%) exhibited predominantly nucleolar MUS81, which co-localized

poorly with SLX4 (Figure 2F). Both control and WEE1i-treated cells showed similar levels of the S-phase marker PCNA (Figure 2G).

In cells treated with WEE1i, just 3 hrs after release from G1/S, a small fraction of the population (~3%) displayed early mitosis features, such as condensed chromatin and bright MUS81 foci that co-localized with SLX4, TOPBP1 and γ-H2AX (Figure S2E, data not shown). In these cells, the number of MUS81 foci was 2-3 fold higher than in control cells with similarly condensed DNA (collected 9 hrs after G1/S release) (Figure S2E and F). This suggests that in cells that are close to completing DNA replication, inhibition of WEE1 licenses recruitment of MUS81-SLX4 to a moderate number of under-replicated chromosomal regions.

MUS81-SLX4 association during S-phase leads to chromosome pulverization and halts DNA replication

Since WEE1 inhibition at the onset of S-phase caused recruitment of active MUS81 to chromosomes, we anticipated it would be highly deleterious to DNA replication. To test this prediction, also supported by previous work (Beck et al., 2010; Beck et al., 2012; Dominguez-Kelly et al., 2011), we released synchronized cells to undergo S-phase in the presence of WEE1i and used flow cytometry to monitor DNA content at 2-hr intervals. Cells treated with WEE1i initiated DNA replication with similar kinetics to DMSO-treated cells. However, whereas control cells completed DNA replication 6-8 hrs after release from G1/S, cells lacking WEE1 activity appeared to arrest bulk DNA synthesis shortly after initiation, displaying a persistent ~3C DNA content (Figure 3A and B).

If WEE1 inhibition leads to impaired DNA replication through toxic cleavage of RFs, we would expect a direct link between premature MUS81-SLX4 association and DNA breakage. Indeed, western-blot analysis of γ-H2AX and KAP1 phosphorylation indicated prompt activation of the DNA-damage response just 2 hrs after cells were released to undergo S-phase in the presence of WEE1i (Figure 3C). Parallel analysis of MUS81-FLAP IPs confirmed that the occurrence of DNA damage correlated tightly with the timing of MUS81-SLX4 complex formation and the inhibition of DNA replication (Figure 3A and D). Interestingly, binding of EME1 and EME2 to

MUS81 did not significantly change throughout the cell cycle or in response to WEE1 inhibition (Figure 3D, Figure S1D). Hence, both non-catalytic subunits might contribute to the WEE1i-triggered DNA damage.

Our results led us to hypothesize that the uncontrolled actions of MUS81-SLX4 on replication intermediates should result in widespread chromosomal breakage. Therefore, we monitored the consequences of WEE1 inhibition on the morphology of metaphase chromosomes in surface spreads. Whereas control cells showed intact chromosomes with sporadic DNA lesions, 94% of cells treated with WEE1i exhibited chromosomes with a pulverized appearance (Figure 3E and F). The remaining fraction of WEE1i-treated cells (6%) displayed non-pulverized chromosomes that nevertheless contained a 30-fold increase in DNA lesions (breaks and radial chromosomes) compared to untreated cells (Figure 3E and F). The two populations of metaphase spreads (pulverized vs. damaged) are likely to reflect MUS81-SLX4 recruitment to early or late S-phase chromosomes (widespread vs. increased foci, respectively) (Figure 2F, S2E and F). Chromosome pulverization triggered by WEE1i was also observed in asynchronous HeLa cultures. Here, the fraction of pulverized metaphases was lower and increased with time, likely reflecting the asynchronous passage through S-phase (Figure S3A).

The unusually high levels of DNA breakage caused by WEE1 inhibition could be confirmed by in situ immunofluorescence analysis of γ-H2AX, which displayed a pan-nuclear distribution in cells released to undergo S-phase in the presence of WEE1i (Figure S2G). Furthermore, analysis of chromosome integrity using pulsed-field gel electrophoresis (PFGE) revealed that more than 65% of all chromosomal DNA was fragmented after just 5 hrs of WEE1 inhibition (Figure 3G).

DNA fragmentation upon WEE1 inhibition is not caused by RPA exhaustion or induction of apoptosis

The excessive accumulation of RPA at stalled replication forks has been shown to precede widespread DNA damage, in a process controlled by the checkpoint kinase ATR (Toledo et al., 2013). Since WEE1 has been suggested to prevent excessive origin firing during S-phase (Beck et al., 2012), we sought to determine whether

exhaustion of RPA precedes DNA breakage in cells treated with WEE1i. Analysis of γ-H2AX and RPA levels by quantitative image-based cytometry (QIBC) (Toledo et al., 2013) showed that WEE1i treatment induced MUS81-EME2-dependent accumulation of DNA damage, without significantly affecting the levels of chromatin-bound RPA (Figure 3H and I, Figure S3B and C). In contrast, control cells treated with HU and ATRi displayed elevated levels of γ-H2AX with concomitant exhaustion of cellular RPA, as previously shown (Figure 3H and I, Figure S3B)(Toledo et al., 2013).

Since chromosome fragmentation is also known to occur during programmed cell death (Nagata et al., 2003), we examined if cells treated with WEE1i showed signs of apoptosis. Western-blot analysis of Caspase 3 and PARP integrity showed no evidence for their proteolytic cleavage within the timeline of chromosomes pulverization (Figure S3D, data not shown).

WEE1 suppresses CDK1 and PLK1-dependent MUS81-SLX4 complex formation to prevent pulverization of S-phase chromosomes

Since CDK1 and PLK1 activities were required for timely MUS81-SLX4 association (Figure 2D), we predicted that inactivation of either kinase should restore DNA replication after WEE1 inhibition. Indeed, FACS analysis revealed that CDK1 and PLK1 inhibitors fully restored the bulk of DNA synthesis in cells released to undergo S-phase in the presence of WEE1i (Figure 4A, data not shown). Furthermore, over 70% of cells co-treated with WEE1i and CDK1 or PLK1 inhibitors displayed intact chromosomes (Figure 4B and C).

In contrast to previous models postulating that WEE1 inhibition causes DNA damage due to excessive activity of the S-phase kinase CDK2 (Beck et al., 2012; Dominguez-Kelly et al., 2011), these data rather suggest that the vast majority of DNA breakage is triggered by premature activation of the mitotic kinases CDK1 and PLK1.

EME2 collaborates with MUS81-SLX4 in processing replication intermediates upon WEE1 inhibition

To verify if chromosome pulverization caused by WEE1 inhibition depends on MUS81-SLX4 nuclease, we monitored DNA damage in cells transfected with siRNAs targeting MUS81, SLX1 or SLX4. Indeed, chromosome spreads, PFGE and western blot analysis of KAP1 phosphorylation revealed a marked reduction in DNA breakage upon MUS81 or SLX4 depletion (Figure 4D and E, S4A). Simultaneous depletion of SLX4 and MUS81 did not show additive effects, suggesting that both are components of the same RF-processing pathway (Figure 4D, data not shown). By contrast, SLX1 depletion did not significantly alter DNA breakage after WEE1 inactivation (Figure 4D and S4A). Importantly, expression of siRNA-resistant catalytically inactive MUS81 (D307A) did not restore DNA damage and chromosome fragmentation in cells depleted of endogenous MUS81 (Figure S4B-D). This establishes that MUS81 nuclease is directly involved in generating DNA lesions upon inhibition of WEE1.

Next, we investigated if EME1 and EME2 contribute to the toxic processing of replication intermediates. siRNAs targeting EME2 almost entirely suppressed chromosome breakage in HeLa cells (Figure 4D, E and S4A) and DNA damage signaling in RPE1-hTERT cultures (Figure S4E). We were unable to determine the relative importance of EME1 using this approach since the tested siRNAs caused elevated levels of cell death upon synchronization (data not shown). To circumvent this problem, we obtained HAP1 cell lines carrying frame-shift mutations in *EME1, EME2* or *MUS81* (Figure S4F, see Note 1 in Extended Experimental Procedures describing evidence for the existence of two isoforms of MUS81: MUS81 and $MUS81_{short}$). We then treated subconfluent cultures of each cell line with WEE1i, and measured DNA damage by PFGE and western-blot analysis of γ-H2AX and KAP1 phosphorylation. Cells lacking *EME1* showed reduced levels of DNA damage induction (Figure 4F and S4G), indicating that EME1 contributes to the efficient cleavage of replication intermediates upon WEE1 inhibition. However, cells lacking EME1 showed a substantial reduction in MUS81 levels, unlike cells lacking EME2 (Figure 4F). Hence, EME1 may promote DNA damage indirectly, through stabilization of the cellular pool of MUS81 protein.

These data suggest that MUS81, EME2 and SLX4, but not SLX1 or $MUS81_{short}$, are components of a protein complex whose premature assembly promotes deleterious breakage of replicating chromosomes.

Inactivation of MUS81 improves cell survival after WEE1 inhibition

Since WEE1 inhibition caused extensive DNA damage, we asked whether cells with pulverized chromosomes would be capable of undergoing cell division. To test this, we used time-lapse microscopy in cells expressing histone H2B-mCherry (Schmitz et al., 2010). Cells treated with WEE1i failed to align chromosomes in a metaphase plate, showed signs of chromosome fragmentation, failed to undergo efficient chromosome segregation and after a prolonged M-phase eventually exited mitosis without dividing (Figure 5A and B, Movie S1). Depletion of EME2 or SLX4 significantly restored chromosome morphology, along with chromosome segregation and cell division (Figure 5A and B, Movie S1, data not shown).

WEE1i (MK-1775) has been shown to selectively sensitize cancer cells to DNA-damaging agents and is in phase II trials for treatment of a broad range of tumors (Aarts et al., 2012; Hirai et al., 2009). Since MUS81-EME2-SLX4 contributes to several phenotypes associated with loss of WEE1 function, we determined whether cellular mortality caused by WEE1i was MUS81-EME2-SLX4-dependent. To monitor short-term cell death in HAP1 cells we used time-lapse microscopy to follow their morphology. After 22 hrs of treatment with WEE1i, ~85% of parental HAP1 cells displayed apoptotic bodies, membrane blebbing and loss of motility. In contrast, cells lacking MUS81 or EME2 showed a significantly higher survival rate (Figure 5C, data not shown). To confirm these data, we followed long-term cell survival using a clonogenic assay. In agreement with the short-term data, WEE1i reduced colony formation in a MUS81 and EME2-depedent manner (Figure 5D).

We next examined cell viability in Fanconi Anemia patient cell lines (FA-P) lacking SLX4 expression (Kim et al., 2013). Similar to HAP1 or HeLa cells, FA-P cells complemented with a vector carrying *SLX4-WT* were significantly more sensitive to increasing concentrations of WEE1i than cells transduced with an empty vector (Figure 5E). Crucially, complementation with a truncated SLX4 version that lacks the

SAP domain (Kim et al., 2013), did not restore sensitivity to WEE1i (Figure 5E). This indicates that SLX4 interaction with MUS81 is important for its role in triggering cell death in response to WEE1 inhibition.

We conclude that MUS81-EME2-SLX4 contributes to cell death after WEE1 inhibition, suggesting that an intact MUS81-EME2-SLX4 pathway may be an important requirement for successful usage of WEE1 inhibitors in the clinic.

Inhibition of DNA replication by MUS81-EME2-SLX4 licenses premature entry into mitosis

The replication arrest caused by WEE1 inactivation raised the intriguing possibility that widespread cleavage of replication intermediates may drive premature entry into mitosis, a hallmark feature of cells with impaired WEE1 function (Heald et al., 1993; Russell and Nurse, 1987)(Figure 3B). To test this model we first examined whether inhibition of PLK1 or depletion of MUS81-EME2-SLX4 restored DNA replication in cells treated with WEE1i. Indeed, as discussed above, FACS analysis of DNA content revealed that PLK1 inhibitors reestablished normal S-phase progression (Figure 4A). Albeit with a slight delay, depletion of MUS81, SLX4 or EME2 also reproducibly restored DNA replication (Figure S5A). The level of rescue was proportional to the reduction in chromosome breakage observed by PFGE (Figure 4D), with EME2 depletion efficiently restoring the bulk of DNA synthesis.

Having created conditions in which DNA replication takes place in the presence of unrestrained CDK1 activity, we next examined whether a temporal intersection between DNA replication and mitosis would occur. Remarkably, inhibition of PLK1 or depletion of MUS81-EME2-SLX4 delayed the onset of mitosis in cells treated with WEE1i (Figure 6A-E, Figure S5B, Movie S2). For EME2 depletion or PLK1 inhibition a near-complete rescue of mitotic entry timing was observed. To further investigate this model, we treated asynchronous HeLa cultures with WEE1i and monitored cell cycle stage distribution using QIBC. Consistent with the results from synchronized cells, a 3-hr treatment with WEE1i led to an EME2-dependent accumulation of nuclear Cyclin B in cells with an S-phase DNA content (Figure 6F-H and S6A, C and D). In turn, the premature accumulation of Cyclin B correlated with

pan-nuclear DNA damage, which was equally reduced by depletion of EME2 (Figure 6F-I, S6A-D).

To test our findings in a non-transformed cell line, we studied the consequences of WEE1 inhibition in RPE1-hTERT cells. As in HeLa cells, WEE1 inhibition caused EME2-dependent DNA damage, replication arrest, premature accumulation of Cyclin B and premature cell rounding in cells released from a single thymidine block (Figure S7A). This could also be confirmed in asynchronous populations using QIBC: treatment with WEE1i caused EME2-dependent DNA damage (Figure S7B) and mild but reproducible accumulation of Cyclin B in cells with a mid and late S-phase DNA content (Figure S7C-F, data not shown).

Overall, these data suggest that suppression of CDK1 activity during S-phase prevents MUS81-EME2-SLX4-mediated premature entry into M-phase.

WEE1 suppresses EME2-dependent activation of CDK1 during S-phase

We next asked whether MUS81-EME2-SLX4 was required for premature CDK1 activation upon inhibition of WEE1. To this end, we monitored the impact of EME2 depletion on the phosphorylation of CDC27, a well-characterized substrate of CDK1 (Peters et al., 1996). Inhibition of WEE1 impaired DNA replication in control cells and led to premature modification of CDC27, which coincided with the detection of DNA damage (KAP1-P) (Figure 7A and B). Notably, depletion of EME2 was sufficient to delay phosphorylation of CDC27 until the bulk of DNA synthesis was completed, approximately 6 hrs after release from G1/S (Figure 7A and B). Nevertheless, phosphorylation of CDC27 still occurred prematurely in cells lacking EME2, presumably due to unrestrained activation of CDK1 in cells that completed DNA replication and transitioned into G2 (Figure 7B).

ATR-independent inhibition of mitotic entry by ongoing DNA replication

Previous work established that the checkpoint kinase ATR prevents premature mitosis during unperturbed growth to ensure sufficient DNA replication (Eykelenboom et al.,

2013). Hence, we suspected the delay in CDK1 activation caused by depletion of EME2, in cells treated with WEE1i, might be ATR-mediated. However, three lines of evidence argued against this model. First, western-blot analysis of CHK1 (S345) and RPA (S33) phosphorylation revealed that WEE1 inhibition alone caused robust activation of ATR, despite triggering premature entry into mitosis (Figure 7B). Second, depletion of EME2, which restored DNA replication, robustly reduced CHK1 and RPA phosphorylation while DNA replication was ongoing (Figure 7A and B). Third, chemical inhibition of ATR -or ATR and ATM combined- did not drastically advance the onset of mitosis in cells treated with WEE1i and depleted of EME2 (Figure 7C and D). Hence, while our data suggest that ATR is active in the absence of WEE1 activity, ATR activity does not appear to suffice in preventing entry into mitosis if replication intermediates are cleaved by MUS81 nuclease.

DISCUSSION

A mechanism for targeted breakage of replication intermediates during mitosis

Previous studies revealed a key role for MUS81 endonuclease in the resolution of stalled replication intermediates at the onset of mitosis (Naim et al., 2013; Ying et al., 2013). However, whether and how cells prevent MUS81 from cleaving vital DNA structures during unperturbed S-phase was unclear. The present work establishes that MUS81 is biochemically able to process model RFs at all stages of the cell cycle, but requires association with SLX4 for efficient substrate targeting in vivo. Since MUS81-SLX4 association is controlled by CDK1-mediated phosphorylation of SLX4, MUS81 is actively targeted to replication intermediates only after the bulk of DNA replication is completed. Therefore, by coupling MUS81-SLX4 association to mitotic entry, cells achieve the selective cleavage of replication intermediates that fail to activate the DNA replication checkpoint. This dynamic regulation prevents stalled replication intermediates from impairing chromosome segregation, while enabling functional replication forks to drive DNA replication during S-phase (Figure 8A and B).

WEE1 prevents unscheduled processing of vital replication intermediates by precluding exposure of S-phase chromosomes to MUS81-SLX4

Our work demonstrates that MUS81 plays a significant role in triggering cell death upon treatment with the WEE1 inhibitor MK-1775. We find that MUS81 is important for the drug to be fully effective in triggering cell death in different cancer cell lines, and provide important new insight into its precise mechanism of action. WEE1 inhibition causes premature activation of the cell cycle kinases CDK1 and PLK1, resulting in unscheduled MUS81-SLX4 association. This exposes replicating chromosomes to MUS81-SLX4 nuclease, triggering cleavage of vital replication intermediates. Therefore, rather than directly inhibiting MUS81 activity as previously suggested (Dominguez-Kelly et al., 2011), we propose that WEE1 prevents DNA breakage by suppressing CDK1 activity prior to the completion of DNA replication (Figure 8B).

Impaired WEE1 function was reported to cause excessive origin firing and nucleotide shortage, followed by MUS81-dependent DNA damage (Beck et al., 2012; Dominguez-Kelly et al., 2011). This led to a model in which WEE1 inhibition causes remodeling of RFs, converting them into MUS81 substrates (Beck et al., 2012). We show that EME2 depletion and PLK1 inhibition efficiently restore the bulk of DNA replication in cells treated with WEE1 inhibitors, arguing that a significant fraction of replication intermediates targeted for cleavage is capable of supporting DNA synthesis effectively. Therefore, even though most naturally-occurring MUS81 substrates are likely to be stalled RFs (Beck et al., 2012; Naim et al., 2013; Neelsen et al., 2013; Ying et al., 2013), we envision that RF remodeling may not be a pre-requisite for substrate recognition and cleavage. In agreement with this model, WEE1 inhibition triggers massive DNA breakage and chromosome pulverization without significantly altering the recruitment of RPA to replicating chromosomes (Figure 3H and I). The data described here does not exclude the possibility that MUS81-mediated cleavage of replication intermediates may not be solely responsible for the cessation of DNA replication in cells treated with WEE1 inhibitors. It is conceivable, for example, that the breakage of a fraction of replication intermediates triggers premature entry into M-phase and nuclear envelope disassembly, which could further contribute to the inhibition of DNA replication.

Besides targeting MUS81 to stalled replication intermediates, SLX4 regulates HJ processing by coordinating the active sites of MUS81 and SLX1 nucleases (Castor et al., 2013; Wyatt et al., 2013). Accordingly, WEE1 activity also prevented premature

MUS81-EME1-SLX1-SLX4 complex formation (Figure S1D). Hence, besides precluding the toxic processing of replication intermediates, WEE1 is likely to play an important role in restricting resolution of recombination intermediates to late stages of the cell cycle. In yeast, analogous suppression of Mus81-Mms4 function during S-phase plays a critical role in preventing the formation of crossover recombinants and in suppressing loss of heterozygosity (Matos et al., 2013; Szakal and Branzei, 2013; Wild and Matos, 2016).

Making DNA replication and mitosis mutually exclusive and ordered

To explain how cells order S-phase and mitosis, Stern and Nurse have put forward a quantitative model for CDK control (Stern and Nurse, 1996). S-phase is initiated when CDK activity increases from a very low to a moderate level, whereas a further increase to high CDK activity initiates mitosis. Accordingly, up-regulation of CDK1 activity during S-phase, by Cyclin B over-expression or WEE1 inactivation, drives mitotic entry prior to the completion of DNA replication (Coudreuse and Nurse, 2010; Moore et al., 2003; Russell and Nurse, 1987). Our work suggests that CDK1 up-regulation during S-phase drives premature entry into mitosis partly due to the untimely assembly of a nuclease capable of halting DNA replication: MUS81-SLX4. When WEE1 is inhibited in cells lacking MUS81-SLX4, DNA replication is significantly restored and mitotic entry shows a concurrent delay. Therefore, we envision that by keeping CDK1 and MUS81-SLX4 in check, WEE1 prevents disappearance of a signal, likely generated by replication intermediates, that inhibits M-phase entry.

In agreement with work in yeast (Magiera et al., 2014), our data raise the interesting possibility that RFs, the target of MUS81-SLX4, negatively regulate M-phase entry by delaying CDK1 activation (Figure 8B). Once DNA replication is completed, the inhibitory signal disappears, allowing CDK1 activity levels to rise. In turn, CDK1 activity licenses MUS81-SLX4 assembly, which resolves any remaining replication intermediates. This double-negative feedback loop warrants that DNA replication and mitosis are mutually exclusive. Furthermore, in conjunction with CDK1 regulators such as WEE1, it ensures that DNA replication temporally precedes mitosis (Figure 8B).

A mechanism for chromosome pulverization and chromothripsis?

It has been suggested that one underlying reason for the temporal separation of DNA replication and mitosis, in eukaryotic cells, is that DNA replication and chromosome condensation might be incompatible (Nasmyth, 1995; Stern and Nurse, 1996). It has also been proposed that, as a consequence of premature compaction, limited chromosome pulverization can occur if a micronucleated cell enters mitosis with an under-replicated micronucleus (Crasta et al., 2012). These findings are relevant for human health since they provide insights into the phenomenon of chromothripsis (Liu et al., 2011; Stephens et al., 2011).

In light of the present work, we would like to suggest a complementary explanation to the incompatibility between DNA replication and mitosis, which takes into account a straightforward mechanism to achieve chromosome pulverization: MUS81-SLX4 cleaves replication intermediates that fail to inhibit mitotic entry. The strength of such model in explaining previous observations related to chromosome shattering events that precede chromothripsis (Forment et al., 2012) is at least four-fold: 1) it is compatible with shattering of a single or multiple chromosomes (e.g. if a single chromosome is found in in a micronucleus, only this chromosome will lag in DNA replication and become a target of MUS81); 2) the level of chromosome breakage is dependent on how under-replicated the particular chromosome is; 3) if more than one chromosome is under-replicated, inter-chromosomal translocations can occur; 4) CDK1 and PLK1, which act as timers of MUS81-SLX4 assembly, are misregulated in a multitude of cancers (Lee et al., 2015; Malumbres and Barbacid, 2009) and therefore replicating chromosomes in these cancer cells may be frequently exposed to the severing actions of MUS81-SLX4.

EXPERIMENTAL PROCEDURES

All experimental procedures are described in detail in the Supplemental Information.

Cell assays

RPE1-hTERT, HAP1, HeLa FRT/TO and HeLa Kyoto cells were maintained in DMEM supplemented with 10% FBS. FA-P cells were maintained in DMEM supplemented with 20% FBS. For siRNA-mediated protein depletion, cells were plated to ~30% confluency, 10-12 hr prior to transfection. The efficiency of protein

depletion was monitored by western blotting 44-60 hrs after transfection. HeLa Kyoto cells stably expressing MUS81-FLAP (CLJM6) (Matos et al., 2011) or SLX4-FLAP (CLJM59) (this study) were generated using BAC recombineering. Cells expressing SLX4-FLAP show a G2/M-specific increase in MUS81 levels (data not shown). This is caused by stabilization of MUS81 by interaction with the additional SLX4-FLAP protein, which is G2/M specific.

To follow the progression of G1/S arrested cells into mitosis, cells were synchronized with a double thymidine block (15-16 hrs) and released into pre-warmed medium. Unless otherwise indicated, MK-1775 (WEE1i) was used at a final concentration of 500 nM.

Short-term and long-term cell survival assays

HAP1 cells were treated with MK-1775 and followed by time-lapse microscopy. Short-term cell survival was calculated by determining the fraction of living cells to the total number of cells in the first and last frame of the movie and expressed as %. Long-term survival of HAP1 cells was determined using a clonogenic assay. Cells were treated for 6 hrs with MK-1775 at final concentrations from 50 nM to 500 nM. After one week, cells were fixed and stained with crystal violet solution. FA-P cells were treated for 6 hrs with MK-1775 at concentrations ranging from 400 to 1200 nM. Cell survival was determined five days later using the Cell Titer-Glo 2.0 reagent (Promega).

Quantitative Image-Based Cytometry

Automated multichannel wide-field microscopy for quantitative image-based cytometry (QIBC) was performed as described (Toledo et al., 2013). Images were acquired either with a 4x or 10x objective under non-saturating conditions. Color-coded scatter plots of asynchronous HeLa and RPE1-hTERT cell populations were generated with Spotfire data visualization software (TIBCO).

Analysis of metaphase chromosomes

Colcemid-treated metaphase cells were spread on microscope slides and chromosomes stained with 7% Giemsa. After washing with water and air-drying overnight, coverslips were mounted on the slides using DPX mounting medium (Merck Millipore) or Permount (Fisher Scientific).

Protein immunoprecipitations

Cells were washed in PBS and lysed in LAP buffer, as previously described (Matos et al., 2011). Cleared lysates were normalized for total protein content and incubated with GFP-Trap matrix (Chromotek) for 90 min at 4°C, followed by extensive washing with LAP buffer.

Nuclease assays

MUS81-FLAP and SLX4-FLAP were semi-purified using GFP-Trap beads. Immunoprecipitates were incubated with 5'-^{32}P- or 5'-^{Cy3}-end-labeled synthetic replication forks or Holliday junctions (Matos et al., 2011). Cleavage products were separated by native PAGE and analyzed by phosphorimaging or fluorescence scanning. Resolution activity (% of cleavage) was calculated as the fraction of nicked duplex DNA product relative to the sum of the intact substrate and resolution product.

Statistical analysis

The number of cells or chromosomes analyzed as well as the number of independent experiments performed is indicated in the figure legends. Error bars on all graphs are SEM or SD. PRISM 6 software (Graphpad) was used for statistical analyzes.

AUTHOR CONTRIBUTIONS

All authors designed and performed experiments and analyzed data. M.Alt. and J.M. supervised the work. J.M. conceived the study and wrote the manuscript. All authors contributed to and proofread the final manuscript.

ACKNOWLEDGMENTS

We thank Steve West for plasmids and antibodies; Agata Smogorzewska for the FA-P cell lines; Daniel Gerlich for the H2B-mCherry cell line; Alessandra Pepe for advice on EME2 depletions; Donat Appert for plasmid construction; Claus Azzalin, Ulrike Kutay, Yves Barral, Boris Pfander and Kai Neelsen for discussions. We thank ScopeM at ETH Zurich and the Center for Microscopy and Image Analysis at UZH for providing imaging facilities. The Blanco lab is supported by Ministerio de Economía y Competitividad and FEDER (RYC-2012-10835 and BFU2013-41554-P). The Altmeyer lab is supported by the Swiss National Science Foundation (Grant PP00P3_150690) and the University of Zurich Association Research Talent Development Fund. The Matos lab is supported by ETH Zürich and the Swiss National Science Foundation (Grants 31003A_153058 and 155823). Jiradet Gloggnitzer is supported by an ETH postdoctoral fellowship (FEL-43 15-2). Philipp Wild is supported by an EMBO long-term fellowship (ALTF 475-2015). Federico Teloni is supported by a UZH Candoc PhD fellowship (FK-16-053).

COMPETING INTERESTS

The authors declare that they have no conflict of interests.

SUPPLEMENTAL INFORMATION

Supplemental information includes extended Experimental Procedures, 7 Figures and 2 Movies.

REFERENCES

Aarts, M., Sharpe, R., Garcia-Murillas, I., Gevensleben, H., Hurd, M.S., Shumway, S.D., Toniatti, C., Ashworth, A., and Turner, N.C. (2012). Forced mitotic entry of S-phase cells as a therapeutic strategy induced by inhibition of WEE1. Cancer discovery *2*, 524-539.
Beck, H., Nahse, V., Larsen, M.S., Groth, P., Clancy, T., Lees, M., Jorgensen, M., Helleday, T., Syljuasen, R.G., and Sorensen, C.S. (2010). Regulators of cyclin-dependent kinases are crucial for maintaining genome integrity in S phase. The Journal of cell biology *188*, 629-638.
Beck, H., Nahse-Kumpf, V., Larsen, M.S., O'Hanlon, K.A., Patzke, S., Holmberg, C., Mejlvang, J., Groth, A., Nielsen, O., Syljuasen, R.G.*, et al.* (2012). Cyclin-dependent kinase suppression by WEE1 kinase protects the genome through control of replication initiation and nucleotide consumption. Mol Cell Biol *32*, 4226-4236.
Castor, D., Nair, N., Declais, A.C., Lachaud, C., Toth, R., Macartney, T.J., Lilley, D.M., Arthur, J.S., and Rouse, J. (2013). Cooperative Control of Holliday Junction Resolution and DNA Repair by the SLX1 and MUS81-EME1 Nucleases. Mol Cell *52*, 221-233.
Coudreuse, D., and Nurse, P. (2010). Driving the cell cycle with a minimal CDK control network. Nature *468*, 1074-1079.
Crasta, K., Ganem, N.J., Dagher, R., Lantermann, A.B., Ivanova, E.V., Pan, Y., Nezi, L., Protopopov, A., Chowdhury, D., and Pellman, D. (2012). DNA breaks and chromosome pulverization from errors in mitosis. Nature *482*, 53-58.
Dominguez-Kelly, R., Martin, Y., Koundrioukoff, S., Tanenbaum, M.E., Smits, V.A., Medema, R.H., Debatisse, M., and Freire, R. (2011). Wee1 controls genomic stability during replication by regulating the Mus81-Eme1 endonuclease. The Journal of cell biology *194*, 567-579.
Enoch, T., and Nurse, P. (1991). Coupling M phase and S phase: controls maintaining the dependence of mitosis on chromosome replication. Cell *65*, 921-923.
Eykelenboom, J.K., Harte, E.C., Canavan, L., Pastor-Peidro, A., Calvo-Asensio, I., Llorens-Agost, M., and Lowndes, N.F. (2013). ATR activates the S-M checkpoint during unperturbed growth to ensure sufficient replication prior to mitotic onset. Cell reports *5*, 1095-1107.
Fekairi, S., Scaglione, S., Chahwan, C., Taylor, E.R., Tissier, A., Coulon, S., Dong, M.Q., Ruse, C., Yates, J.R., 3rd, Russell, P.*, et al.* (2009). Human SLX4 is a Holliday junction resolvase subunit that binds multiple DNA repair/recombination endonucleases. Cell *138*, 78-89.
Forment, J.V., Blasius, M., Guerini, I., and Jackson, S.P. (2011). Structure-specific DNA endonuclease Mus81/Eme1 generates DNA damage caused by Chk1 inactivation. PloS one *6*, e23517.
Forment, J.V., Kaidi, A., and Jackson, S.P. (2012). Chromothripsis and cancer: causes and consequences of chromosome shattering. Nature reviews. Cancer *12*, 663-670.
Gallo-Fernandez, M., Saugar, I., Ortiz-Bazan, M.A., Vazquez, M.V., and Tercero, J.A. (2012). Cell cycle-dependent regulation of the nuclease activity of Mus81-Eme1/Mms4. Nucleic acids research *40*, 8325-8335.
Gritenaite, D., Princz, L.N., Szakal, B., Bantele, S.C., Wendeler, L., Schilbach, S., Habermann, B.H., Matos, J., Lisby, M., Branzei, D.*, et al.* (2014). A cell

cycle-regulated Slx4-Dpb11 complex promotes the resolution of DNA repair intermediates linked to stalled replication. Genes Dev *28*, 1604-1619.
Guervilly, J.H., Takedachi, A., Naim, V., Scaglione, S., Chawhan, C., Lovera, Y., Despras, E., Kuraoka, I., Kannouche, P., Rosselli, F.*, et al.* (2015). The SLX4 complex is a SUMO E3 ligase that impacts on replication stress outcome and genome stability. Mol Cell *57*, 123-137.
Hanada, K., Budzowska, M., Davies, S.L., van Drunen, E., Onizawa, H., Beverloo, H.B., Maas, A., Essers, J., Hickson, I.D., and Kanaar, R. (2007). The structure-specific endonuclease Mus81 contributes to replication restart by generating double-strand DNA breaks. Nature structural & molecular biology *14*, 1096-1104.
Hartwell, L.H., and Weinert, T.A. (1989). Checkpoints: controls that ensure the order of cell cycle events. Science *246*, 629-634.
Heald, R., McLoughlin, M., and McKeon, F. (1993). Human wee1 maintains mitotic timing by protecting the nucleus from cytoplasmically activated Cdc2 kinase. Cell *74*, 463-474.
Hirai, H., Iwasawa, Y., Okada, M., Arai, T., Nishibata, T., Kobayashi, M., Kimura, T., Kaneko, N., Ohtani, J., Yamanaka, K.*, et al.* (2009). Small-molecule inhibition of Wee1 kinase by MK-1775 selectively sensitizes p53-deficient tumor cells to DNA-damaging agents. Molecular cancer therapeutics *8*, 2992-3000.
Jackson, S.P., and Bartek, J. (2009). The DNA-damage response in human biology and disease. Nature *461*, 1071-1078.
Jin, P., Hardy, S., and Morgan, D.O. (1998). Nuclear localization of cyclin B1 controls mitotic entry after DNA damage. The Journal of cell biology *141*, 875-885.
Kim, Y., Spitz, G.S., Veturi, U., Lach, F.P., Auerbach, A.D., and Smogorzewska, A. (2013). Regulation of multiple DNA repair pathways by the Fanconi anemia protein SLX4. Blood *121*, 54-63.
Lee, K.S., Burke, T.R., Jr., Park, J.E., Bang, J.K., and Lee, E. (2015). Recent Advances and New Strategies in Targeting Plk1 for Anticancer Therapy. Trends Pharmacol Sci *36*, 858-877.
Liu, P., Erez, A., Nagamani, S.C., Dhar, S.U., Kolodziejska, K.E., Dharmadhikari, A.V., Cooper, M.L., Wiszniewska, J., Zhang, F., Withers, M.A.*, et al.* (2011). Chromosome catastrophes involve replication mechanisms generating complex genomic rearrangements. Cell *146*, 889-903.
Magiera, M.M., Gueydon, E., and Schwob, E. (2014). DNA replication and spindle checkpoints cooperate during S phase to delay mitosis and preserve genome integrity. The Journal of cell biology *204*, 165-175.
Malumbres, M., and Barbacid, M. (2009). Cell cycle, CDKs and cancer: a changing paradigm. Nature reviews. Cancer *9*, 153-166.
Mankouri, H.W., Huttner, D., and Hickson, I.D. (2013). How unfinished business from S-phase affects mitosis and beyond. EMBO J *32*, 2661-2671.
Matos, J., Blanco, M.G., Maslen, S., Skehel, J.M., and West, S.C. (2011). Regulatory control of the resolution of DNA recombination intermediates during meiosis and mitosis. Cell *147*, 158-172.
Matos, J., Blanco, M.G., and West, S.C. (2013). Cell-cycle kinases coordinate the resolution of recombination intermediates with chromosome segregation. Cell reports *4*, 76-86.

Minocherhomji, S., Ying, S., Bjerregaard, V.A., Bursomanno, S., Aleliunaite, A., Wu, W., Mankouri, H.W., Shen, H., Liu, Y., and Hickson, I.D. (2015). Replication stress activates DNA repair synthesis in mitosis. Nature *528*, 286-290.
Moore, J.D., Kirk, J.A., and Hunt, T. (2003). Unmasking the S-phase-promoting potential of cyclin B1. Science *300*, 987-990.
Munoz, I.M., Hain, K., Declais, A.C., Gardiner, M., Toh, G.W., Sanchez-Pulido, L., Heuckmann, J.M., Toth, R., Macartney, T., Eppink, B.*, et al.* (2009). Coordination of structure-specific nucleases by human SLX4/BTBD12 is required for DNA repair. Mol Cell *35*, 116-127.
Nagata, S., Nagase, H., Kawane, K., Mukae, N., and Fukuyama, H. (2003). Degradation of chromosomal DNA during apoptosis. Cell Death Differ *10*, 108-116.
Naim, V., Wilhelm, T., Debatisse, M., and Rosselli, F. (2013). ERCC1 and MUS81-EME1 promote sister chromatid separation by processing late replication intermediates at common fragile sites during mitosis. Nature cell biology *15*, 1008-1015.
Nasmyth, K. (1995). Evolution of the cell cycle. Philosophical transactions of the Royal Society of London. Series B, Biological sciences *349*, 271-281.
Neelsen, K.J., Zanini, I.M., Herrador, R., and Lopes, M. (2013). Oncogenes induce genotoxic stress by mitotic processing of unusual replication intermediates. The Journal of cell biology *200*, 699-708.
Pedersen, R.T., Kruse, T., Nilsson, J., Oestergaard, V.H., and Lisby, M. (2015). TopBP1 is required at mitosis to reduce transmission of DNA damage to G1 daughter cells. The Journal of cell biology *210*, 565-582.
Pepe, A., and West, S.C. (2014a). MUS81-EME2 Promotes Replication Fork Restart. Cell reports *7*, 1048-1055.
Pepe, A., and West, S.C. (2014b). Substrate specificity of the MUS81-EME2 structure selective endonuclease. Nucleic acids research *42*, 3833-3845.
Peters, J.M., King, R.W., Hoog, C., and Kirschner, M.W. (1996). Identification of BIME as a subunit of the anaphase-promoting complex. Science *274*, 1199-1201.
Pines, J. (1999). Four-dimensional control of the cell cycle. Nature cell biology *1*, E73-79.
Russell, P., and Nurse, P. (1987). Negative regulation of mitosis by wee1+, a gene encoding a protein kinase homolog. Cell *49*, 559-567.
Schmitz, M.H., Held, M., Janssens, V., Hutchins, J.R., Hudecz, O., Ivanova, E., Goris, J., Trinkle-Mulcahy, L., Lamond, A.I., Poser, I.*, et al.* (2010). Live-cell imaging RNAi screen identifies PP2A-B55alpha and importin-beta1 as key mitotic exit regulators in human cells. Nature cell biology *12*, 886-893.
Stephens, P.J., Greenman, C.D., Fu, B., Yang, F., Bignell, G.R., Mudie, L.J., Pleasance, E.D., Lau, K.W., Beare, D., Stebbings, L.A.*, et al.* (2011). Massive genomic rearrangement acquired in a single catastrophic event during cancer development. Cell *144*, 27-40.
Stern, B., and Nurse, P. (1996). A quantitative model for the cdc2 control of S phase and mitosis in fission yeast. Trends in genetics : TIG *12*, 345-350.
Svendsen, J.M., Smogorzewska, A., Sowa, M.E., O'Connell, B.C., Gygi, S.P., Elledge, S.J., and Harper, J.W. (2009). Mammalian BTBD12/SLX4 assembles a Holliday junction resolvase and is required for DNA repair. Cell *138*, 63-77.

Szakal, B., and Branzei, D. (2013). Premature Cdk1/Cdc5/Mus81 pathway activation induces aberrant replication and deleterious crossover. EMBO J *32*, 1155-1167.
Techer, H., Koundrioukoff, S., Carignon, S., Wilhelm, T., Millot, G.A., Lopez, B.S., Brison, O., and Debatisse, M. (2016). Signaling from Mus81-Eme2-Dependent DNA Damage Elicited by Chk1 Deficiency Modulates Replication Fork Speed and Origin Usage. Cell reports.
Toledo, L.I., Altmeyer, M., Rask, M.B., Lukas, C., Larsen, D.H., Povlsen, L.K., Bekker-Jensen, S., Mailand, N., Bartek, J., and Lukas, J. (2013). ATR prohibits replication catastrophe by preventing global exhaustion of RPA. Cell *155*, 1088-1103.
Wild, P., and Matos, J. (2016). Cell cycle control of DNA joint molecule resolution. Curr Opin Cell Biol *40*, 74-80.
Wyatt, H.D., Sarbajna, S., Matos, J., and West, S.C. (2013). Coordinated actions of SLX1-SLX4 and MUS81-EME1 for Holliday junction resolution in human cells. Mol Cell *52*, 234-247.
Ying, S., Minocherhomji, S., Chan, K.L., Palmai-Pallag, T., Chu, W.K., Wass, T., Mankouri, H.W., Liu, Y., and Hickson, I.D. (2013). MUS81 promotes common fragile site expression. Nature cell biology *15*, 1001-1007.
Zhou, B.B., and Elledge, S.J. (2000). The DNA damage response: putting checkpoints in perspective. Nature *408*, 433-439.

FIGURE LEGENDS:

Figure 1. MUS81 is active during S-phase and targeted to under-replicated regions by SLX4 during mitosis. See also Figures S1 and S2.

(A) HeLa cells expressing MUS81-FLAP were released from a double thymidine block. MUS81-FLAP immunoprecipitates (IPs) were analyzed by western blotting and for RF-processing activity. * indicates 5´-labeling. See Note 1 in Extended Experimental Procedures describing evidence for two isoforms of MUS81: MUS81 and $MUS81_{short.}$

(B) Quantification of mitotic index and RF processing activity of MUS81-FLAP from (A). Substrate cleavage was normalized to MUS81 protein levels.

(C) DNA content analysis of cells from (A) and (B) by FACS.

(D) MUS81-FLAP was immunoprecipitated from control or SLX1-depleted HeLa cells synchronized with thymidine (Thy) or nocodazole (Noc). IPs were analyzed as in (A).

(E) Immunofluorescence (IF) analysis of SLX4-FLAP, MUS81, TOPBP1 and γ-H2AX in HeLa cells. Nucleoplasmic proteins were pre-extracted.

(F) Distribution of SLX4-FLAP foci number in individual prometaphase cells from (E), quantified from three independent experiments (mean ± SD, n>90 cells).

(G) IF analysis of MUS81 localization at prometaphase in cells treated with the indicated siRNAs.

(H) Distribution of MUS81 foci in individual prometaphase cells from (G), quantified from three independent experiments (mean ± SD, n>90 cells/condition).

(I) Mean number of MUS81 foci per prometaphase cell and frequency of colocalization with TOPBP1 from (G) (± SEM), quantified from 3 (>90 prometaphase cells) and 2 (>50 TOPBP1-positive cells) independent experiments.

Figure 2. WEE1 inhibition elicits CDK1 and PLK1-dependent recruitment of active MUS81-SLX4 nuclease to S-phase chromosomes. See also Figure S2.

(A) Schematic representation of human SLX4 with the domains required for interaction with XPF (blue), MUS81 (brown) and SLX1 (orange). The approximate relative position of all minimal CDK1 consensus sites (S/TP) is depicted. Residues in red are phosphorylated in vivo (source: http://www.phosphosite.org).

(B) HeLa cells were transfected with the indicated vectors to express FLAG-tagged $SLX4^{WT}$ or $SLX4^{41A}$ and synchronized at prometaphase with nocodazole. Cell lysates and anti-FLAG immunoprecipitates were analyzed for the indicated proteins.

(C) HeLa cells were transfected with the indicated vectors and treated and analyzed as in (B). $SLX4^{6A}$ has Alanine substitutions at T1524, T1544, T1561, T1571, T1676 and S1681. $SLX4^{35A}$ has Alanine substitutions in all S/TP sites not mutated in $SLX4^{6A}$.

(D) HeLa cells expressing SLX4-FLAP were released from a double thymidine block in the presence of DMSO, MK-1775 (WEE1i), WEE1i + RO-3306 (CDK1i) or WEE1i + BI2536 (PLK1i). SLX4-FLAP IPs were analyzed for the indicated proteins and for RF-processing activity. * indicates 5´-labeling.

(E) Quantification of the mitotic index and RF processing activity from (D). RF-processing activity of MUS81-FLAP IPs from Figure S2D is plotted for comparison. Substrate cleavage was normalized to SLX4 or MUS81 protein levels.

(F) Representative images of MUS81 and SLX4-FLAP localization 3 hr after release from single thymidine block and quantification of MUS81 localization (nucleolar vs. pan-nuclear foci). Pan-nuclear MUS81 foci were found in 7 ± 0.53% (control) and 95 ± 1.45% (WEE1i-treated) of all interphase cells (mean ± SEM; n> 200; 3 independent experiments).

(G) PCNA was stained and visualized as in (F). PCNA localization was quantified from two independent experiments (n>200 cells/condition).

Figure 3. WEE1 restrains MUS81-SLX4 association during S-phase to prevent pulverization of replicating chromosomes. See also Figure S3.

(A) HeLa cells expressing MUS81-FLAP were released from a double thymidine block in the presence or absence of WEE1i. DNA content was analyzed by FACS. A direct comparison of the DNA content of three samples at the indicated time points is shown (right panel).

(B) Mitotic index (%) of cells synchronized as in (A).

(C) Soluble extracts prepared from samples collected in (A) were analyzed by western blotting.

(D) MUS81-FLAP IPs from extracts prepared as in (C) were analyzed by western blotting.

(E) Representative images of metaphase spreads prepared from cells treated as in (A) 10 hr after thymidine release.

(F) Quantification of chromosomal morphologies in (E), n=169. The data corresponds to a single experiment but identical results were observed in 6 independent experiments.

(G) HeLa cells were synchronized and treated as in (A). Samples were collected 5 hr after release and DNA analyzed by PFGE.

(H) Asynchronous HeLa cells were treated with HU (2mM) and ATR inhibitor AZ-20 (1μM) to induce replication catastrophe, or with WEE1i, pre-extracted, stained for γ-H2AX and RPA, and analyzed by quantitative image-based cytometry. Color-code: Mean γ-H2AX levels.

(I) Bar chart depicting cell population averages of chromatin-bound RPA from (H).

Figure 4. CDK1 and PLK1 promote MUS81-EME2-SLX4-dependent chromosome pulverization in the absence of WEE1 activity. See also Figure S4.

(A) HeLa cells were released from a double thymidine block in the presence of DMSO or the indicated inhibitors. DNA content was analyzed by FACS.

(B) Metaphase spreads of cells treated as in (A) were prepared 6 hr after release from thymidine block. For each condition, representative images and frequency of pulverized metaphases are shown.

(C) Cells were treated as in (A). Samples were collected 5 hr after release and DNA was analyzed by PFGE. The ratio of broken to total DNA was quantified from three experiments (mean ± SEM).

(D) Synchronized HeLa cells, siRNA-depleted for the indicated proteins, were collected and analysed by PFGE as in (C).

(E) Metaphase spreads of cells treated as in (D) were prepared 6 or 8 hr after release from the second thymidine block. Representative images are shown. Frequency of pulverized metaphases was determined from three independent experiments (mean ± SD). "Non-pulverized" chromosomes were either intact or displayed moderate levels of DNA breakage.

(F) Subconfluent HAP1 cells with the indicated genotypes were cultured in the absence or presence of WEE1i for 14 hr. Soluble extracts were analyzed for the indicated proteins. * indicates an unspecific signal.

Figure 5. WEE1 suppresses MUS81-EME2-SLX4-dependent cell death. See also Movie S1.

(A) HeLa cells expressing H2B-mCherry, siRNA-depleted for the indicated proteins, were released from a double thymidine block in the presence of WEE1i. Time-lapse microscopy was used to follow cellular and chromatin morphologies. Metaphase plate formation was quantified in cells that had undergone mitotic cell rounding. Representative DIC and H2B-mCherry images are shown. >100 cells were analyzed for each condition.

(B) Nuclear division was analyzed and quantified from reattaching cells in (A) (n>50 per condition). Representative images are shown.

(C) Survival of asynchronous HAP1 cells of the indicated genotypes after 22 hr WEE1i treatment was monitored by time-lapse microscopy. The surviving fraction was quantified from three experiments (mean ± SD, n>100 cells / condition).

(D) HAP1 cells of the indicated genotypes were treated with DMSO or WEE1i for 6 hr. Cell survival was monitored with a clonogenic assay. Data points representing the surviving fraction are plotted in a $\log_{10}$ scale and denote mean ± SEM, derived from three replicates (*p< 0.05, two tailed t-test).

(E) Fanconi Anemia patient cells (FA-P) transduced with constructs expressing the indicated versions of SLX4 were treated with DMSO or WEE1i for 6 hr. Cell survival was monitored with a luciferase-based assay. Data points representing the surviving fraction are plotted in log10 scale and denote mean ± SEM, derived from three replicates (*p< 0.05, two tailed t-test).

Figure 6. WEE1 inhibition during S-phase causes MUS81-EME2-SLX4-dependent premature entry into mitosis. See also Figures S5, S6 and Movie S2.

(A) HeLa Kyoto cells were released from a double thymidine block in the presence of the indicated kinase inhibitors. Mitotic cell rounding was monitored by time-lapse microscopy and represented as mitotic index over time. Mitotic entry was defined as first frame in which the cell had fully rounded up.

(B) Box-and-whiskers plots depict median time of mitotic entry of cells in (A); n>50, whiskers represent 95% confidence interval. Asterisks indicate significant differences (*p< 0.05, ****p< 0.0001; two-way ANOVA).

(C) HeLa cells, transfected twice with siRNAs targeting transcripts of the indicated proteins, were released from a double thymidine block in the presence of WEE1i. Cells were analyzed as in (B) (n>50 cells).

(D) HeLa FRT/TO cells conditionally expressing siRNA-resistant MUS81-WT-SF or MUS81-ND-SF were siRNA-depleted for the indicated proteins. 24 hrs after induction of MUS81 expression, cells were released from a double thymidine block in the presence of WEE1i. Cells were analyzed as in (B) (n>50 cells).

(E) HeLa cells, siRNA-depleted for the indicated proteins, were released from a double thymidine block in the presence of WEE1i. Cells were analyzed as in (B) (n>50 cells).

(F) Asynchronously proliferating HeLa cells were treated with siRNAs as indicated, exposed to WEE1i for 3hrs with a 20 minute EdU pulse at the end of the treatment, stained for γ-H2AX, Cyclin B1 and EdU, and analyzed by quantitative image-based cytometry. Scatter plots depict mean EdU intensities versus total nuclear DAPI intensities. Color-code: Mean Cyclin B levels.

(G) Data from (F) plotted to depict mean nuclear Cyclin B levels vs. total nuclear DAPI intensities. Color-code: Mean γ-H2AX levels.

(H) The bar chart depicts mean nuclear Cyclin B levels in cell cycle staged population averages according to their DAPI/EdU profiles in (S6C).

(I) The bar chart depicts mean nuclear γ-H2AX levels in cell cycle staged population averages according to their DAPI/EdU profiles in (S6C).

Figure 7. WEE1- and ATR-independent suppression of CDK1 activity and mitotic entry during S-phase

(A) HeLa cells, transfected with the indicated siRNAs, were released from a double thymidine block in the presence of WEE1i. DNA content was analyzed by FACS.

(B) Protein extracts from cells collected in (A) were analyzed by western blotting.

(C) HeLa cells, siRNA-depleted for EME2, were released from a double thymidine block in the presence of the indicated inhibitors and analyzed as in (A) and (B).

(D) HeLa cells, siRNA-depleted for the indicated proteins, were released from a double thymidine block in the presence of the indicated kinase inhibitors (500 nM WEE1i; 2 μM ATRi (VE-821); 10 μM ATMi (KU-55933). Mitotic cell rounding was monitored by time-lapse microscopy. Box-and-whiskers plots depict median time of mitotic entry. Whiskers represent a 95% confidence interval, n>50 cells. Asterisks indicate significant differences (****p< 0.0001; two-way ANOVA).

Figure 8. A mechanism for controlled breakage of under-replicated chromosomes during mitosis

(A) WEE1 kinase inhibits CDK1 during S-phase, indirectly preventing MUS81-SLX4 association. PLK1 promotes MUS81-SLX4 association but is not essential for complex assembly. During mitosis, multiple MUS81 molecules are bridged by SLX4, which can dimerize (Guervilly et al., 2015). However, it is unclear whether SLX4 dimerization is cell cycle regulated or required for the bridging of MUS81 molecules. MUS81 represents MUS81-EME2 heterodimers.

(B) Working model: a double-negative feedback loop ensures that DNA replication and mitosis are temporally separated. Ongoing DNA replication delays entry into mitosis. In turn, CDK1- and PLK1-dependent assembly of MUS81-SLX4 at the G2/M transition ensures nucleolytic processing of any residual replication intermediates (top panel).

In cells treated with WEE1 inhibitors, premature association of SLX4 and MUS81 promotes chromosome pulverization (middle panel). After depletion of MUS81-EME2 or SLX4, WEE1 inhibition no longer halts the bulk of DNA replication. M-phase entry is concurrently delayed, suggesting that ongoing replication delays the onset of mitosis (bottom panel).

Figure 1

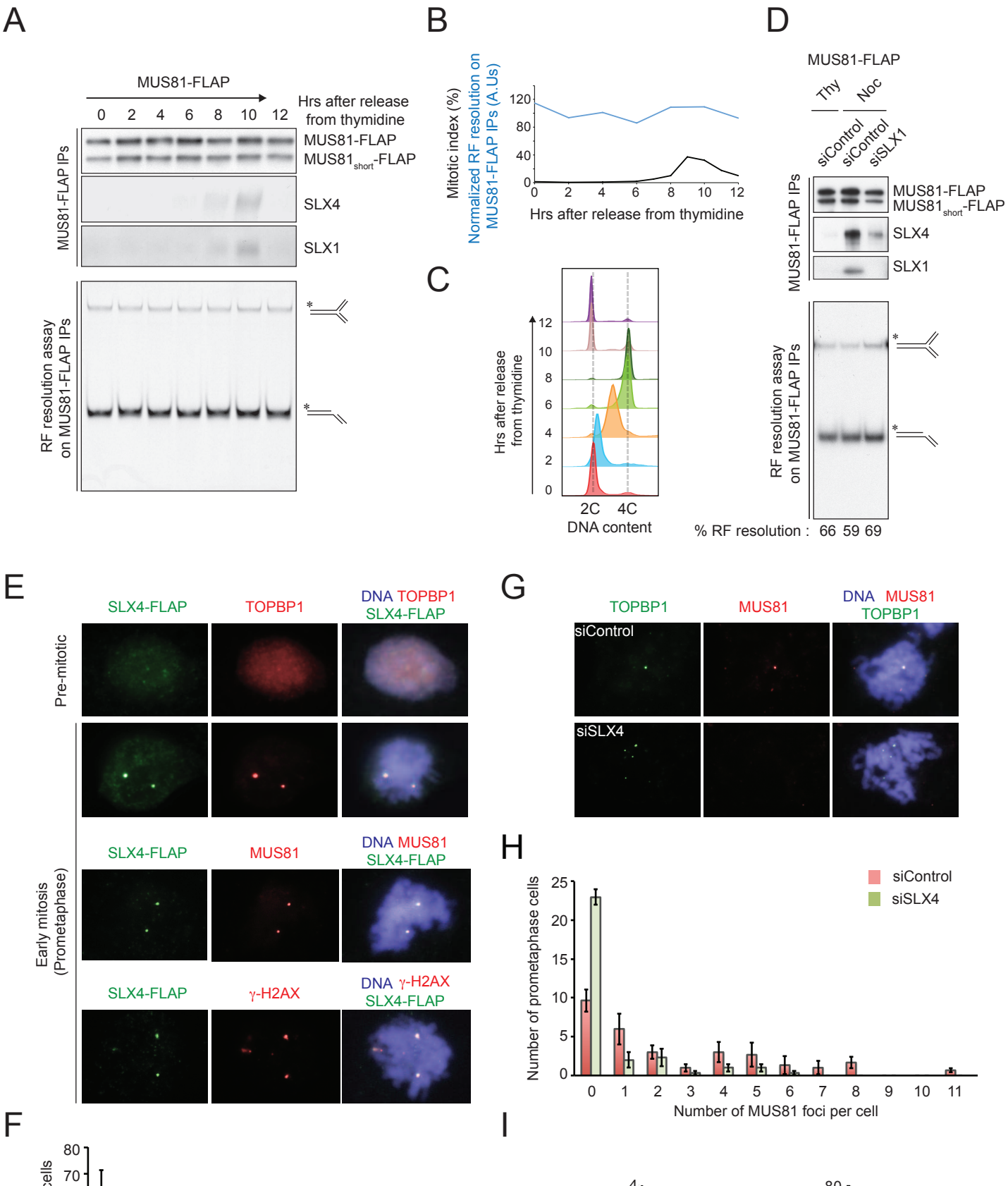
A
MUS81-FLAP
0 2 4 6 8 10 12
Hrs after release from thymidine
MUS81-FLAP IPs
MUS81-FLAP
MUS81short-FLAP
SLX4
SLX1
RF resolution assay on MUS81-FLAP IPs
B
Mitotic index (%)
Normalized RF resolution on MUS81-FLAP IPs (A.Us)
120
80
40
0
0 2 4 6 8 10 12
Hrs after release from thymidine
C
Hrs after release from thymidine
12
10
8
6
4
2
0
2C 4C
DNA content
D
MUS81-FLAP
Thy
Noc
siControl
siControl
siSLX1
MUS81-FLAP IPs
MUS81-FLAP
MUS81short-FLAP
SLX4
SLX1
RF resolution assay on MUS81-FLAP IPs
% RF resolution : 66 59 69
E
SLX4-FLAP
TOPBP1
DNA TOPBP1 SLX4-FLAP
Pre-mitotic
Early mitosis (Prometaphase)
SLX4-FLAP
MUS81
DNA MUS81 SLX4-FLAP
SLX4-FLAP
γ-H2AX
DNA γ-H2AX SLX4-FLAP
G
TOPBP1
MUS81
DNA MUS81 TOPBP1
siControl
siSLX4
H
siControl
siSLX4
Number of prometaphase cells
25
20
15
10
5
0
0 1 2 3 4 5 6 7 8 9 10 11
Number of MUS81 foci per cell
F
Number of prometaphase cells
80
70
60
50
40
30
20
10
0
0 1 2 3 4 5 6 7 8 9 10 11 12 13 14 15
Number of SLX4 foci per cell
I
MUS81 foci per cell
4
3
2
1
0
siControl
siSLX4
TOPBP1 foci that contain MUS81 (%)
80
60
40
20
0
siControl
siSLX4

Figure 2

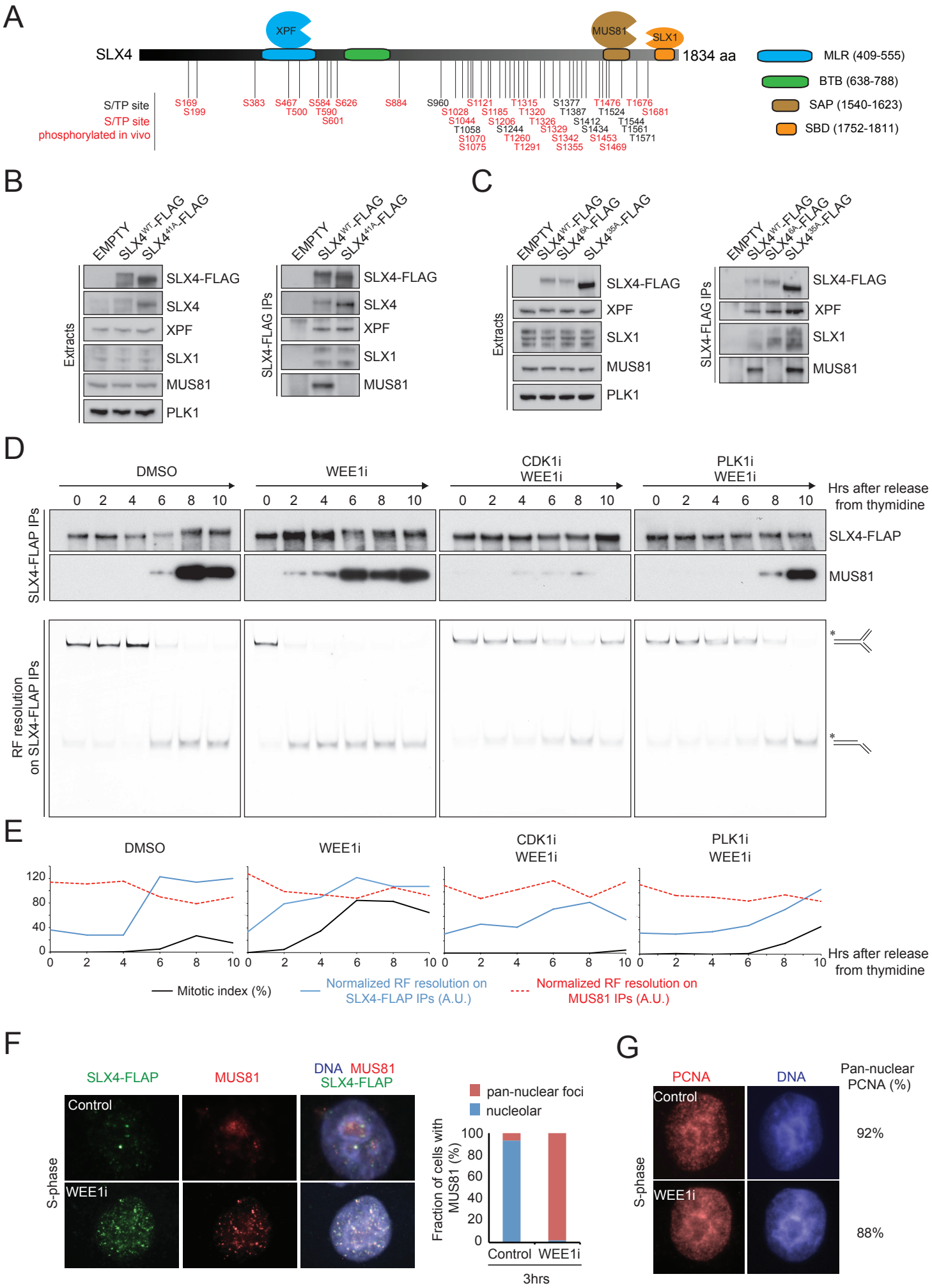
A
XPF
MUS81
SLX1
SLX4
1834 aa
MLR (409-555)
BTB (638-788)
SAP (1540-1623)
SBD (1752-1811)
S/TP site
S/TP site phosphorylated in vivo
S169 S199 S383 S467 T500 S584 S590 S601 S626 S884 S960 S1028 S1044 T1058 S1070 S1075 S1121 S1185 S1206 S1244 T1260 T1291 T1315 T1320 T1326 S1329 S1342 S1355 S1377 T1387 S1412 S1434 S1453 S1469 T1476 T1524 T1544 T1561 T1571 T1676 S1681
B
EMPTY
SLX4WT-FLAG
SLX4 41A-FLAG
Extracts
SLX4-FLAG IPs
SLX4-FLAG
SLX4
XPF
SLX1
MUS81
PLK1
C
EMPTY
SLX4WT-FLAG
SLX4 6A-FLAG
SLX4 35A-FLAG
Extracts
SLX4-FLAG IPs
SLX4-FLAG
XPF
SLX1
MUS81
PLK1
D
DMSO
WEE1i
CDK1i WEE1i
PLK1i WEE1i
0 2 4 6 8 10
Hrs after release from thymidine
SLX4-FLAP IPs
SLX4-FLAP
MUS81
RF resolution on SLX4-FLAP IPs
E
DMSO
WEE1i
CDK1i WEE1i
PLK1i WEE1i
120
80
40
0
0 2 4 6 8 10
Hrs after release from thymidine
Mitotic index (%)
Normalized RF resolution on SLX4-FLAP IPs (A.U.)
Normalized RF resolution on MUS81 IPs (A.U.)
F
SLX4-FLAP
MUS81
DNA MUS81 SLX4-FLAP
Control
WEE1i
S-phase
pan-nuclear foci
nucleolar
Fraction of cells with MUS81 (%)
100
80
60
40
20
0
Control WEE1i
3hrs
G
PCNA
DNA
Pan-nuclear PCNA (%)
Control
WEE1i
S-phase
92%
88%

Figure 3

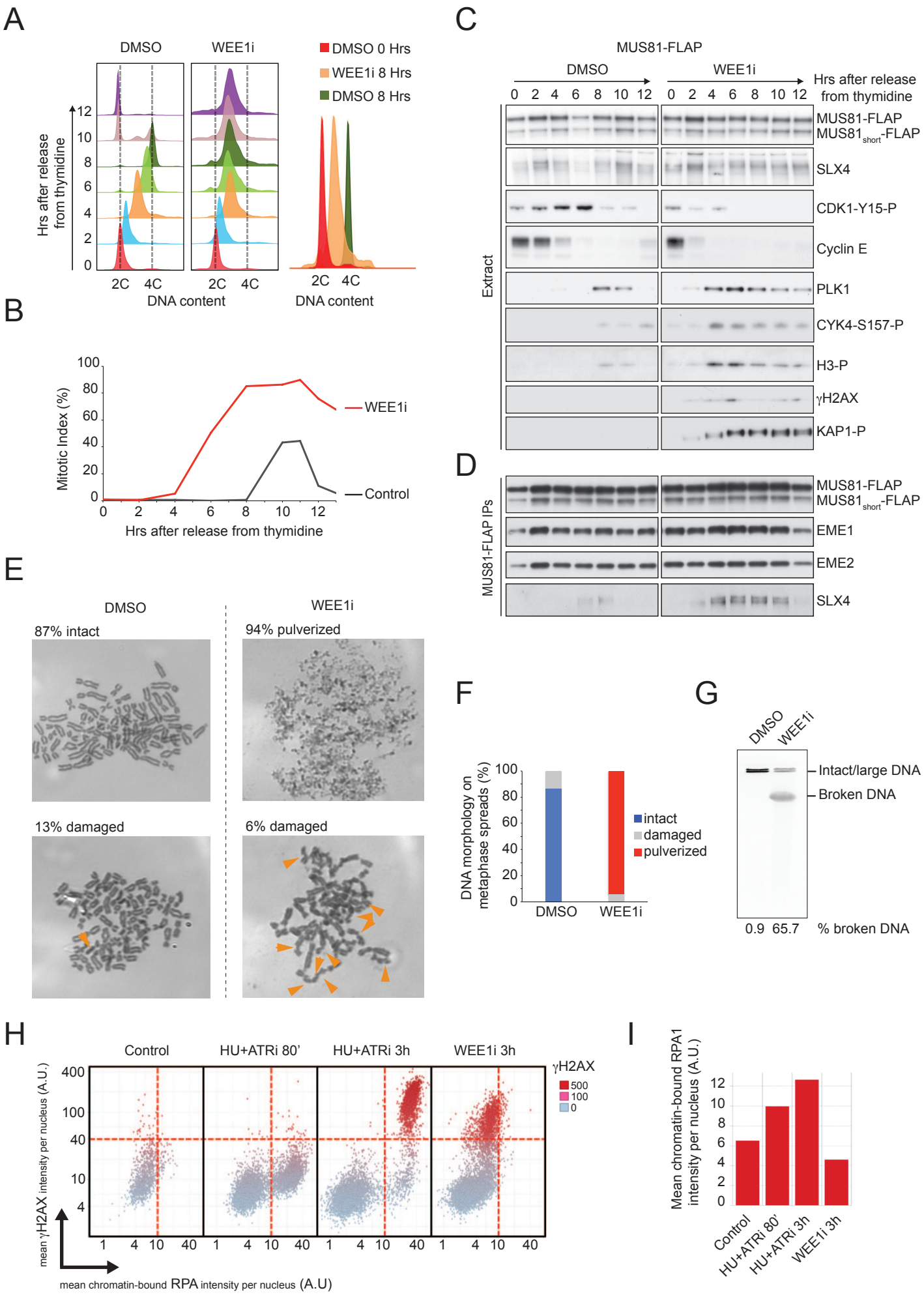
A
DMSO
WEE1i
DMSO 0 Hrs
WEE1i 8 Hrs
DMSO 8 Hrs
Hrs after release from thymidine
12
10
8
6
4
2
0
2C 4C
2C 4C
DNA content
2C 4C
DNA content
B
Mitotic Index (%)
100
80
60
40
20
0
0 2 4 6 8 10 12
Hrs after release from thymidine
WEE1i
Control
C
MUS81-FLAP
DMSO
WEE1i
0 2 4 6 8 10 12
0 2 4 6 8 10 12
Hrs after release from thymidine
Extract
MUS81-FLAP
MUS81short-FLAP
SLX4
CDK1-Y15-P
Cyclin E
PLK1
CYK4-S157-P
H3-P
γH2AX
KAP1-P
D
MUS81-FLAP IPs
MUS81-FLAP
MUS81short-FLAP
EME1
EME2
SLX4
E
DMSO
WEE1i
87% intact
94% pulverized
13% damaged
6% damaged
F
DNA morphology on metaphase spreads (%)
100
80
60
40
20
0
DMSO
WEE1i
intact
damaged
pulverized
G
DMSO
WEE1i
Intact/large DNA
Broken DNA
0.9 65.7
% broken DNA
H
Control
HU+ATRi 80'
HU+ATRi 3h
WEE1i 3h
γH2AX
500
100
0
mean γH2AX intensity per nucleus (A.U.)
400
100
40
10
4
1 4 10 40
mean chromatin-bound RPA intensity per nucleus (A.U)
I
Mean chromatin-bound RPA1 intensity per nucleus (A.U.)
12
10
8
6
4
2
0
Control
HU+ATRi 80'
HU+ATRi 3h
WEE1i 3h

Figure 4

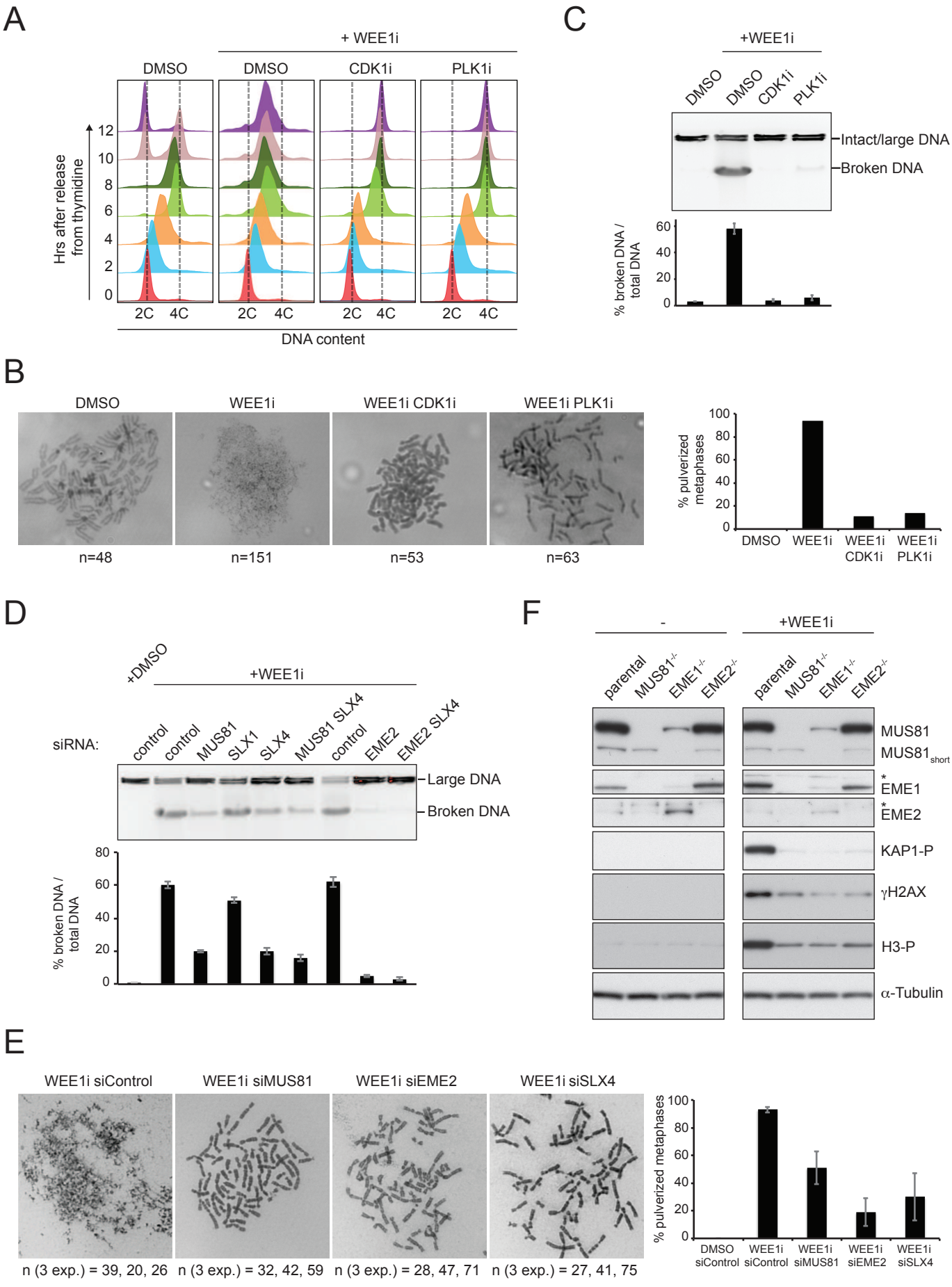
A
+ WEE1i
DMSO
DMSO
CDK1i
PLK1i
Hrs after release from thymidine
12
10
8
6
4
2
0
2C 4C 2C 4C 2C 4C 2C 4C
DNA content
C
+WEE1i
DMSO
DMSO
CDK1i
PLK1i
Intact/large DNA
Broken DNA
% broken DNA / total DNA
60
40
20
0
B
DMSO
WEE1i
WEE1i CDK1i
WEE1i PLK1i
n=48
n=151
n=53
n=63
% pulverized metaphases
100
80
60
40
20
0
DMSO
WEE1i
WEE1i CDK1i
WEE1i PLK1i
D
+DMSO
+WEE1i
siRNA:
control
control
MUS81
SLX1
SLX4
MUS81 SLX4
control
EME2
EME2 SLX4
Large DNA
Broken DNA
% broken DNA / total DNA
80
60
40
20
0
F
-
+WEE1i
parental
MUS81-/-
EME1-/-
EME2-/-
parental
MUS81-/-
EME1-/-
EME2-/-
MUS81
MUS81short
*EME1
*EME2
KAP1-P
γH2AX
H3-P
α-Tubulin
E
WEE1i siControl
WEE1i siMUS81
WEE1i siEME2
WEE1i siSLX4
n (3 exp.) = 39, 20, 26
n (3 exp.) = 32, 42, 59
n (3 exp.) = 28, 47, 71
n (3 exp.) = 27, 41, 75
% pulverized metaphases
100
80
60
40
20
0
DMSO siControl
WEE1i siControl
WEE1i siMUS81
WEE1i siEME2
WEE1i siSLX4

Figure 5

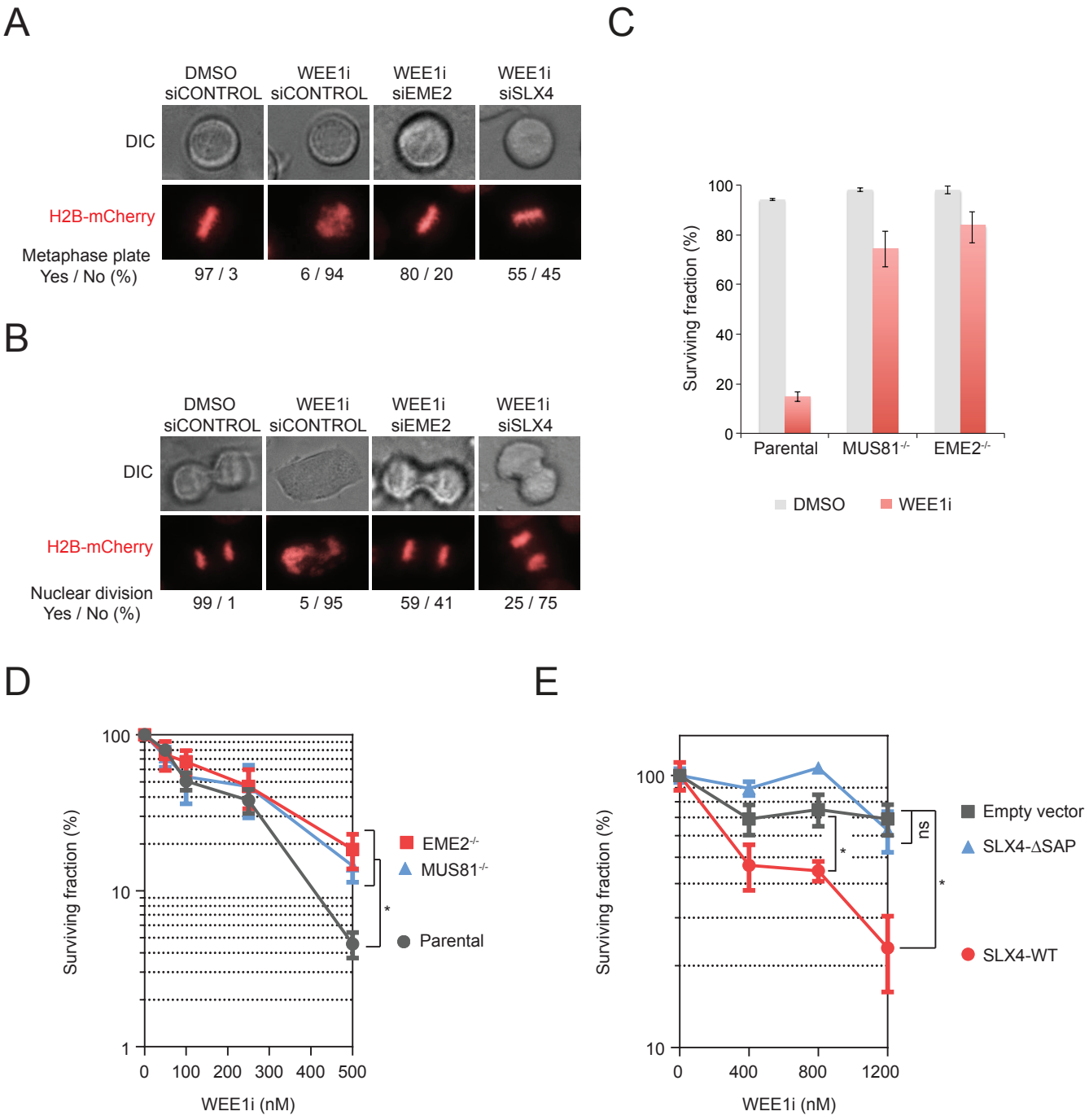
A
DMSO siCONTROL
WEE1i siCONTROL
WEE1i siEME2
WEE1i siSLX4
DIC
H2B-mCherry
Metaphase plate Yes / No (%)
97 / 3
6 / 94
80 / 20
55 / 45
B
DMSO siCONTROL
WEE1i siCONTROL
WEE1i siEME2
WEE1i siSLX4
DIC
H2B-mCherry
Nuclear division Yes / No (%)
99 / 1
5 / 95
59 / 41
25 / 75
C
Surviving fraction (%)
100
80
60
40
20
0
Parental
MUS81-/-
EME2-/-
DMSO
WEE1i
D
Surviving fraction (%)
100
10
1
0
100
200
300
400
500
WEE1i (nM)
EME2-/-
MUS81-/-
Parental
*
E
Surviving fraction (%)
100
10
0
400
800
1200
WEE1i (nM)
Empty vector
SLX4-ΔSAP
SLX4-WT
ns
*
*

Figure 6

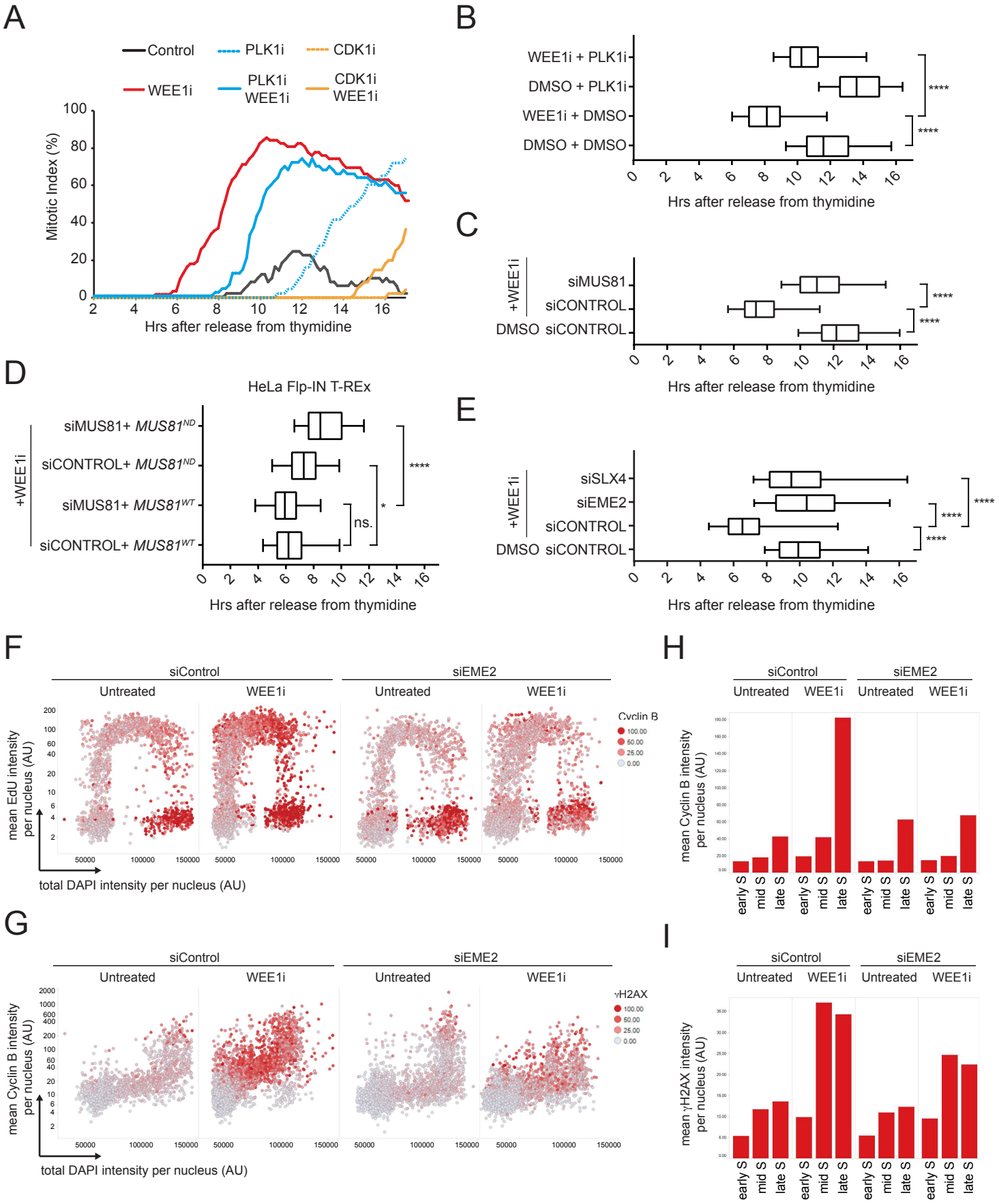
A
Control
PLK1i
CDK1i
WEE1i
PLK1i WEE1i
CDK1i WEE1i
Mitotic Index (%)
Hrs after release from thymidine
B
WEE1i + PLK1i
DMSO + PLK1i
WEE1i + DMSO
DMSO + DMSO
****
****
Hrs after release from thymidine
C
+WEE1i
siMUS81
siCONTROL
DMSO siCONTROL
****
****
Hrs after release from thymidine
D
HeLa Flp-IN T-REx
+WEE1i
siMUS81+ MUS81ND
siCONTROL+ MUS81ND
siMUS81+ MUS81WT
siCONTROL+ MUS81WT
****
*
ns.
Hrs after release from thymidine
E
+WEE1i
siSLX4
siEME2
siCONTROL
DMSO siCONTROL
****
****
****
Hrs after release from thymidine
F
siControl
siEME2
Untreated
WEE1i
Untreated
WEE1i
mean EdU intensity per nucleus (AU)
Cyclin B
100.00
50.00
25.00
0.00
total DAPI intensity per nucleus (AU)
H
siControl
siEME2
Untreated
WEE1i
Untreated
WEE1i
mean Cyclin B intensity per nucleus (AU)
early S
mid S
late S
G
siControl
siEME2
Untreated
WEE1i
Untreated
WEE1i
mean Cyclin B intensity per nucleus (AU)
γH2AX
100.00
50.00
25.00
0.00
total DAPI intensity per nucleus (AU)
I
siControl
siEME2
Untreated
WEE1i
Untreated
WEE1i
mean γH2AX intensity per nucleus (AU)
early S
mid S
late S

Figure 7

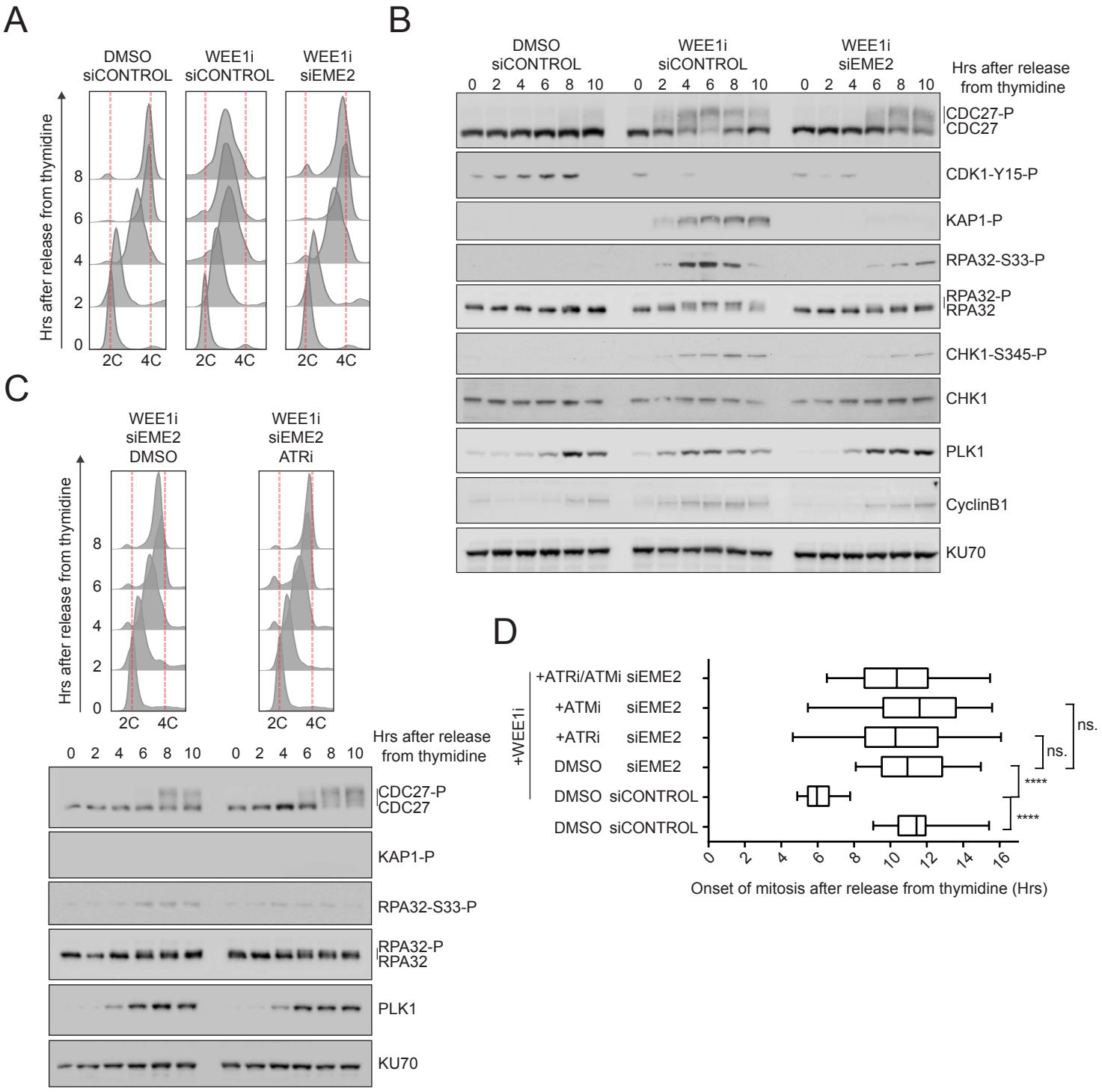
A
DMSO siCONTROL
WEE1i siCONTROL
WEE1i siEME2
Hrs after release from thymidine
0
2
4
6
8
2C
4C
B
DMSO siCONTROL
WEE1i siCONTROL
WEE1i siEME2
0 2 4 6 8 10
Hrs after release from thymidine
CDC27-P
CDC27
CDK1-Y15-P
KAP1-P
RPA32-S33-P
RPA32-P
RPA32
CHK1-S345-P
CHK1
PLK1
CyclinB1
KU70
C
WEE1i siEME2 DMSO
WEE1i siEME2 ATRi
Hrs after release from thymidine
D
+WEE1i
+ATRi/ATMi siEME2
+ATMi siEME2
+ATRi siEME2
DMSO siEME2
DMSO siCONTROL
DMSO siCONTROL
ns.
ns.
****
****
Onset of mitosis after release from thymidine (Hrs)

Figure 8

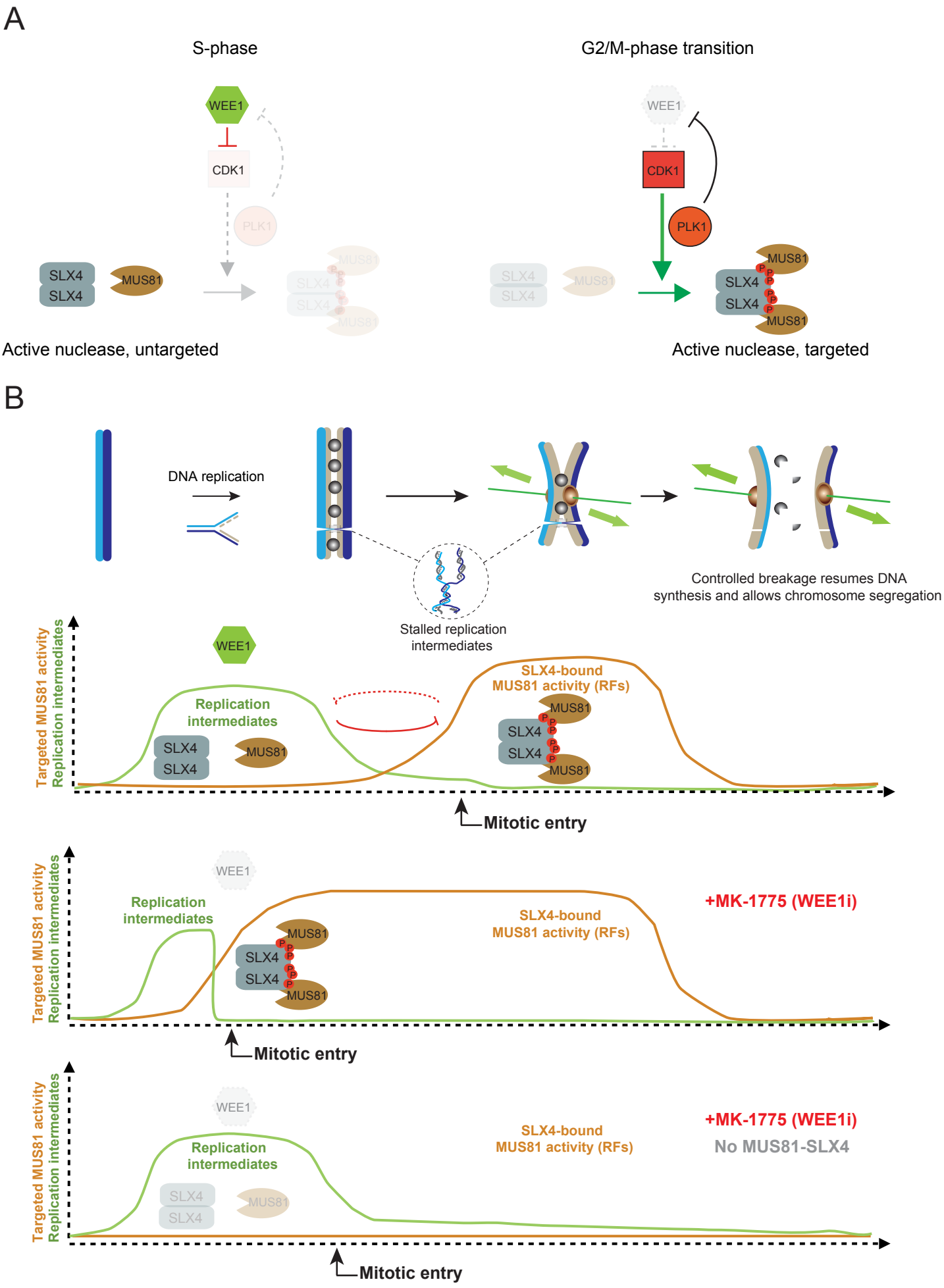
A
S-phase
G2/M-phase transition
WEE1
CDK1
PLK1
SLX4
SLX4
MUS81
Active nuclease, untargeted
Active nuclease, targeted
B
DNA replication
Stalled replication intermediates
Controlled breakage resumes DNA synthesis and allows chromosome segregation
Targeted MUS81 activity
Replication intermediates
SLX4-bound MUS81 activity (RFs)
Mitotic entry
+MK-1775 (WEE1i)
No MUS81-SLX4

Inventory of Supplemental Materials:

SUPPLEMENTAL FIGURES

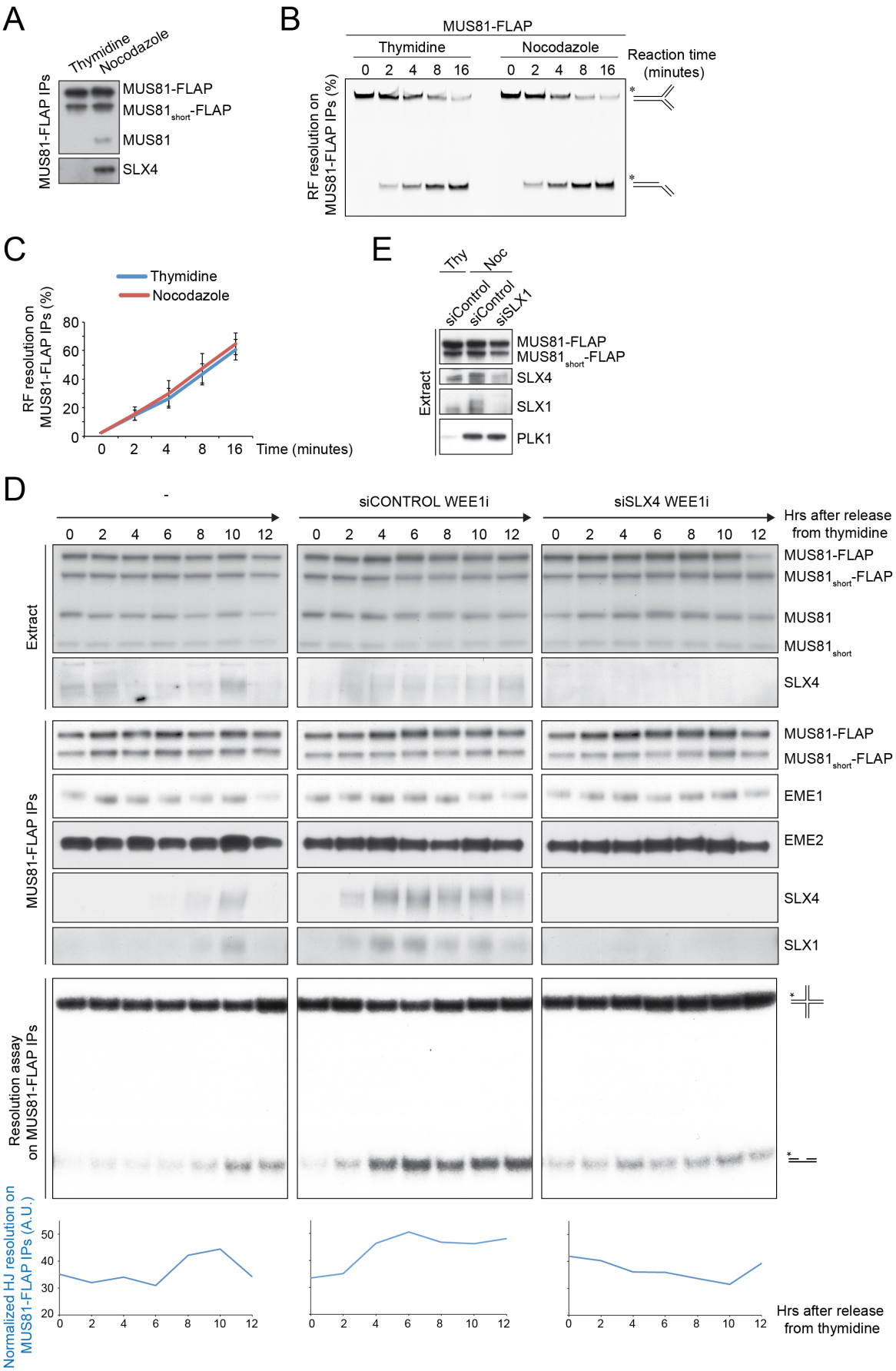

Figure S1. MUS81-associated HJ-processing activity is cell cycle regulated and prematurely enhanced after WEE1 inhibition (Related to Figure 1 and Figure 2)

(A) HeLa cells expressing MUS81-FLAP were synchronized at G1/S with thymidine or at prometaphase with nocodazole. MUS81-FLAP was affinity purified from extracts and analyzed by western blotting for the indicated proteins. **(B)** Immunoprecipiates from **(A)** were split and incubated with a model RF substrate. Cleavage reactions were carried out for the indicated times. * indicates 5´-labelling. **(C)** Quantification and graphical display of the RF-resolution activity from **(B)**. Values were quantified from three independent MUS81-FLAP immunoprecipitations and resolution assays (mean ± SD). **(D)** HeLa cells expressing MUS81-FLAP, treated with no siRNAs, control siRNAs or siRNAs targeting SLX4, were synchronized at G1/S by a double thymidine block and released in the presence of DMSO or MK-1775 (WEE1i). MUS81-FLAP was affinity purified from the extracts and analyzed by western blotting for the presence of the indicated proteins and for HJ-processing activity. * indicates 5´-labelling. Some of the western blots in the left panel are identical to the ones in Figure 1A. HJ resolution was assayed in the same time course samples. Quantification and graphical display of the HJ-resolution activity is shown. Substrate cleavage was normalized to MUS81 protein levels in the IPs. **(E)** Soluble extracts corresponding to Figure 1D. HeLa cells expressing MUS81-FLAP were treated with control siRNAs or siRNAs targeting SLX1, and synchronized with thymidine (Thy) or nocodazole (Noc) for 18 hours. Soluble extracts were analyzed for the indicated proteins by western blotting.

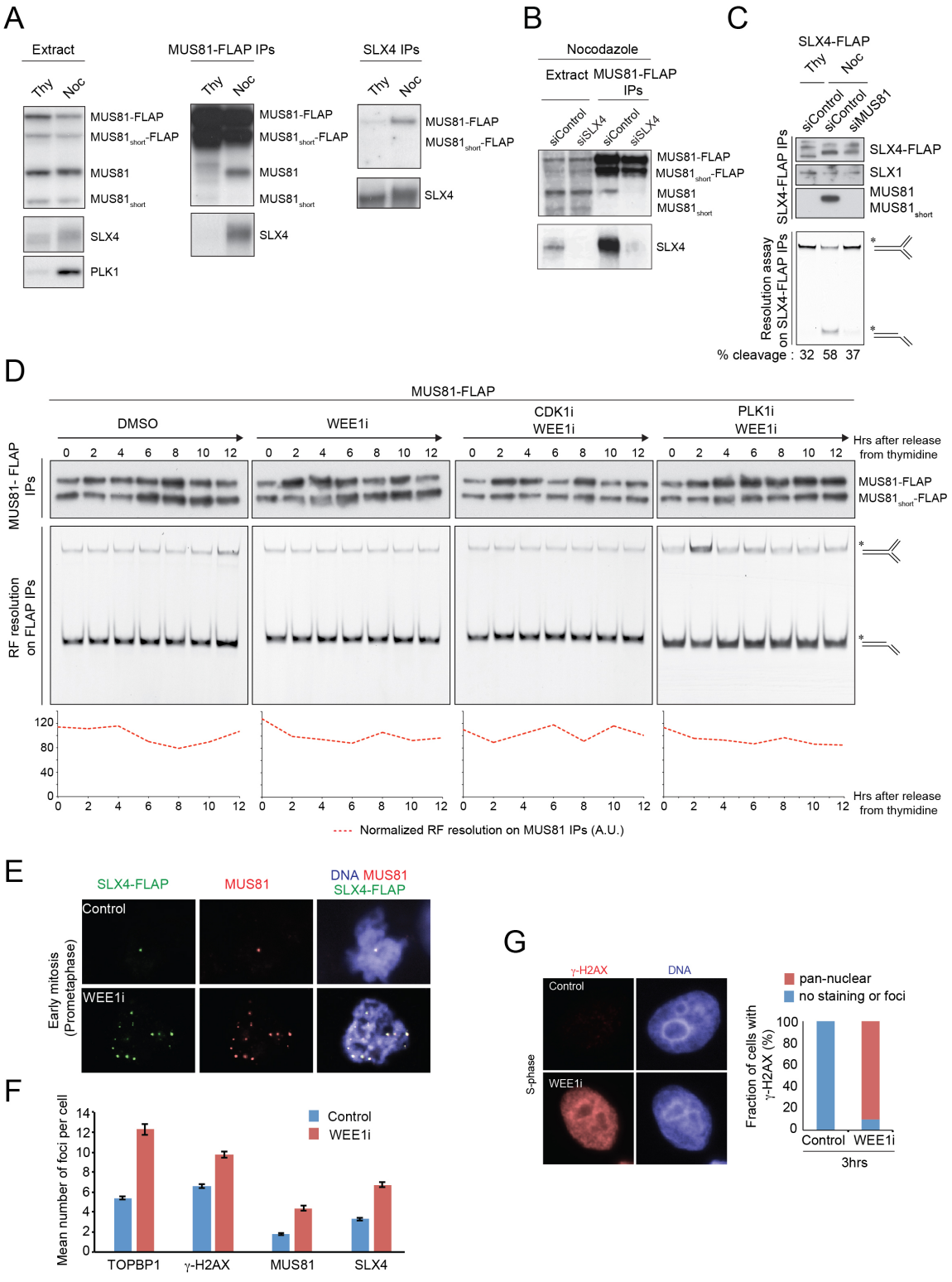

Figure S2. MUS81 nuclease activity on model replication forks is independent of WEE1, CDK1 and PLK1 kinases (Related to Figure 1 and Figure 2)

(A) MUS81-FLAP was affinity-purified from HeLa cells synchronized with thymidine (Thy) or nocodazole (Noc). Soluble extracts, anti-FLAP and anti-SLX4 IPs were analyzed for the indicated proteins. **(B)** HeLa cells expressing MUS81-FLAP treated with control siRNAs or siRNAs targeting SLX4 were synchronized at prometaphase with nocodazole. Soluble extracts and anti-FLAP IPs were analyzed as in **(A)**. **(C)** SLX4-FLAP was affinity-purified from control or MUS81-depleted HeLa cells,

and synchronized with thymidine (Thy) or nocodazole (Noc). IPs were analyzed by western blotting for the indicated proteins and for RF processing activity. * indicates 5´-labeling. **(D)** HeLa cells expressing MUS81-FLAP were synchronized at G1/S by a double thymidine block and released in the presence of DMSO, MK1775 (WEE1i), WEE1i + RO-3306 (CDK1i) or WEE1i + BI2536 (PLK1i). MUS81-FLAP was affinity purified from extracts and analyzed for RF processing activity. * indicates 5´-labelling. Substrate cleavage was normalized to MUS81 protein levels. **(E)** Representative images of SLX4-FLAP and MUS81 localization in prometaphase cells treated as in Figure 2F. Control cells were fixed 9 hr after thymidine release. **(F)** Cells prepared as in **(E)** were stained for SLX4-FLAP, MUS81, TOPBP1 or γ-H2AX. The plotted values represent the mean number of foci per prometaphase cell (± SEM). > 90 cells, pooled from 3 experiments, were analyzed for each staining and for each condition. **(G)** WEE1 prevents widespread DNA damage during S-phase. HeLa cells were synchronized at G1/S by a single thymidine block and released in the absence or presence of MK-1775 (WEE1i). γ-H2AX was stained and analyzed 3 hours after release (S-phase chromosomes). Representative images are shown. 200 cells were analyzed for each condition and γ-H2AX distribution (pan-nuclear vs. no staining/foci) was quantified.

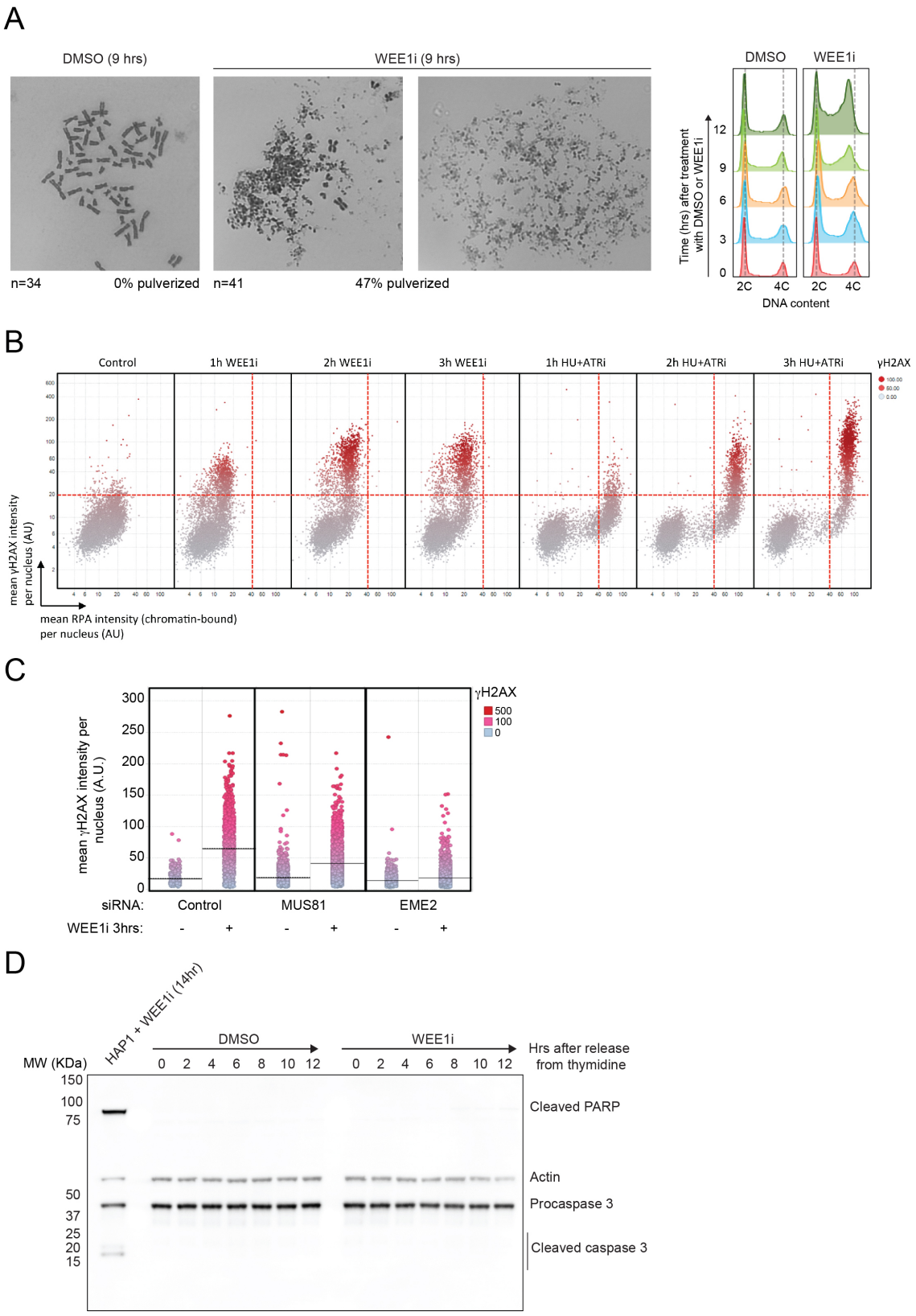

Figure S3. Chromosome pulverization upon WEE1 inhibition is not caused by RPA exhaustion or apoptotic cell death (Related to Figure 3).

(A) Metaphase spreads were prepared from asynchronously proliferating HeLa cells treated for 9 hours with DMSO or WEE1i (500 nM). Representative images of the observed chromosomal morphologies are shown. In a parallel experiment, DNA content was monitored by FACS at the indicated time points

after treatment with DMSO or WEE1i. **(B)** Asynchronously proliferating HeLa cells were treated for the indicated time periods with a combination of HU (2mM) and ATR inhibitor AZ-20 (1μM) to induce replication catastrophe, or with WEE1i (500nM), pre-extracted, stained for γ-H2AX and RPA, and analyzed by quantitative image-based cytometry. Color-code: Mean γ-H2AX levels. **(C)** Asynchronously proliferating HeLa cells, siRNA-depleted for the indicated protein, were treated with WEE1i (500nM) for 3 hours, pre-extracted, stained for γ-H2AX and analyzed by quantitative image-based cytometry. Color-code: Mean γ-H2AX levels. **(D)** HeLa cells were synchronized at G1/S by a double thymidine block and released in the presence of WEE1i. Protein extracts were analyzed by western blotting for the indicated proteins. PARP cleavage and Caspase 3 cleavage are hallmarks of programmed cell death by apoptosis. As a positive control for the visualization of apoptotic markers, HAP1 cells were treated with WEE1i for 14 hours, which results in the death of a significant part of the population (> 80% after 24hr, **Figure 5C**).

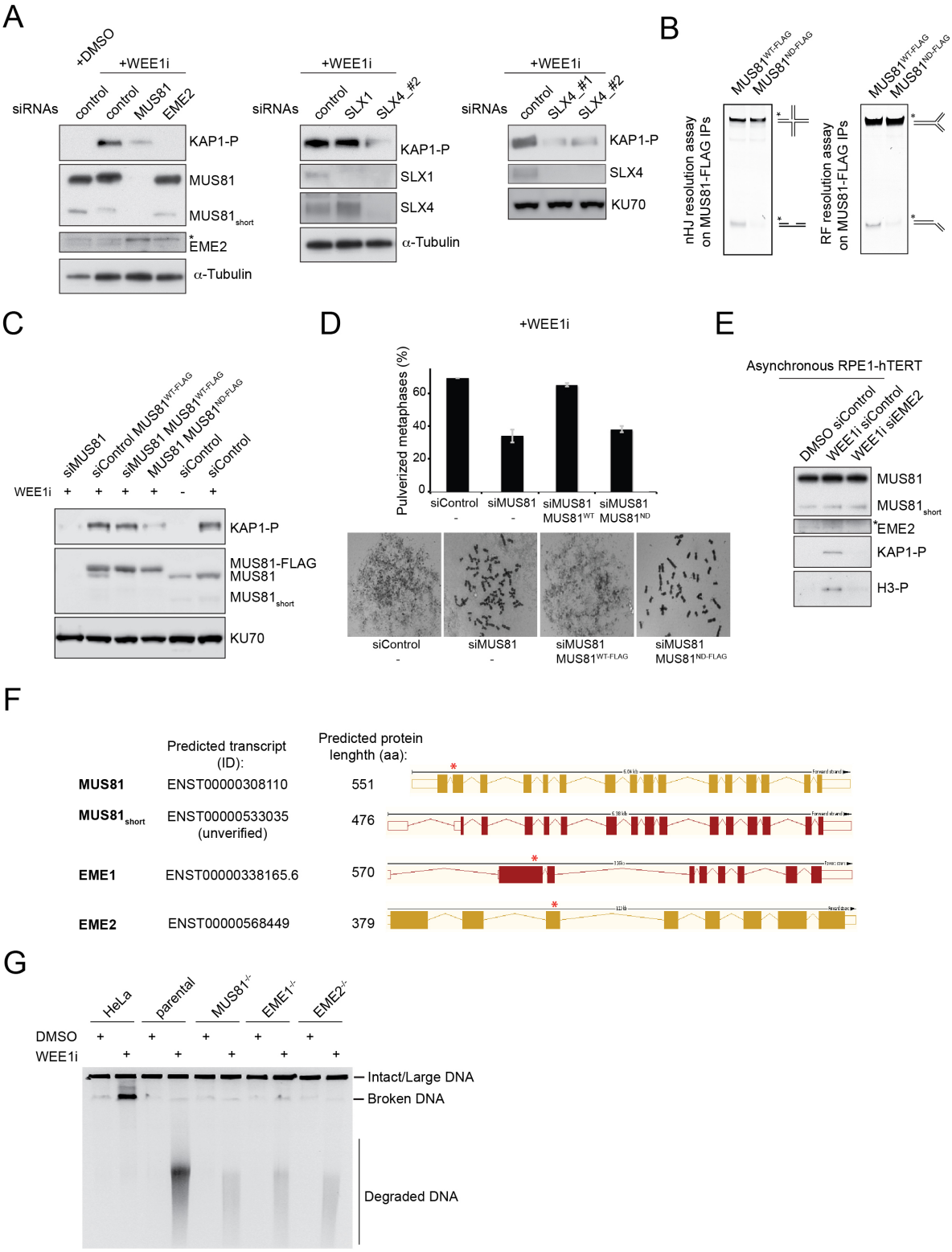

Figure S4. MUS81, EME2 and SLX4-dependent DNA damage after WEE1 inhibition (Related to Figure 4)

(A) HeLa cells, siRNA-depleted for the indicated proteins, were synchronized using a double thymidine block. Samples were collected 5 hours after release and extracts analyzed by western blotting for the indicated proteins. * indicates an unspecific signal. Samples from the same cultures were analyzed by PFGE in Figure 4D. **(B)** HeLa FRT/TO cells conditionally expressing MUS81-WT-SF or MUS81-ND-SF (Nuclease-Dead) were induced for 16 hours. MUS81-SF was affinity-purified

using FLAG-beads and IPs were analyzed for nuclease activity on a nicked HJ (nHJ) or a replication fork (RF) substrate. *indicates 5´-labeling. MUS81-ND contains the D307A mutation, which impairs its catalytic activity. The SF tag is composed of StrepII-FLAG. **(C)** HeLa FRT/TO cells conditionally expressing siRNA-resistant MUS81-WT-SF or MUS81-ND-SF (Nuclease-Dead) were siRNA-depleted for the indicated proteins. 24 hours after induction of MUS81 expression, cells were released from a double thymidine block in the presence or absence of WEE1i. Soluble extracts from samples collected 8 hours after release from G1/S were analyzed by western blotting for the indicated proteins. KU70 was used as a loading control. **(D)** Metaphase spreads were prepared from cells treated as in **(C)**, collected 8 hours after release from the second thymidine block. The frequency of pulverized metaphases is shown (top graph)(mean ± SEM). >100 metaphases were analyzed for each condition in 3 biological replicates. Examples of pulverized vs. intact chromosomes are shown (bottom panel). **(E)** Western blot analysis of protein extracts from asynchronous RPE1-hTERT cells transfected with siRNAs targeting the indicated proteins. DMSO or WEE1i was added to cultures 12 hours prior to sample collection. **(F)** Schematic representation of the consensus transcript for full-length MUS81 and a putative transcript encoding a version of MUS81 that lacks the initial 75 amino-acids, which we have named $MUS81_{short}$. The consensus transcripts for EME1 and EME2 are also shown. (*) marks the approximate positions of frameshift-inducing mutations introduced in HAP1 cells, using CRISPR-Cas9. 1bp insertion in exon 2 that results in the specific disruption of full length MUS81; 10bp deletion in exon 2 disrupts EME1; 1bp deletion in exon 3 disrupts EME2. **(G)** Subconfluent HAP1 cells with the indicated genotypes were cultured in the absence or presence of WEE1i for 12 hours. Samples were collected and DNA was analyzed by PFGE. Note: While DNA breakage upon WEE1 inhibition is strongly dependent on the integrity of MUS81, EME1 and EME2, in HAP1 cells, DNA appears to be further processed, potentially by additional enzymes. MUS81-mediated apoptotic cell death may trigger the additional DNA degradation.

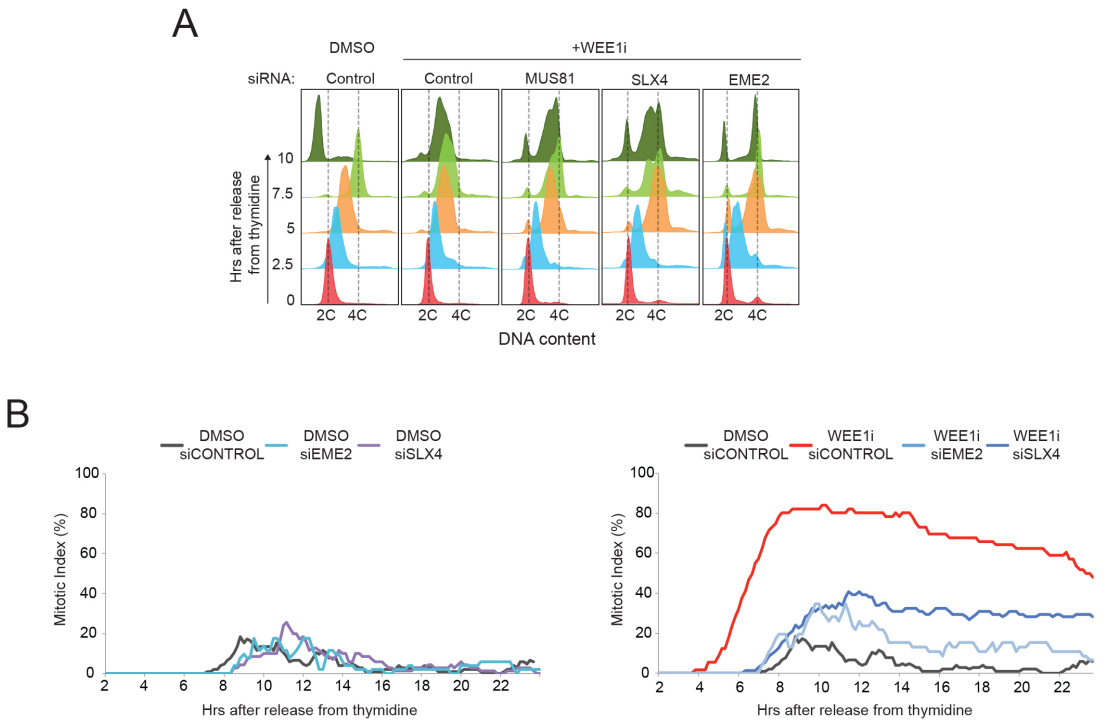

Figure S5. WEE1 inhibition causes premature entry into mitosis in pre-synchronized cells. (Related to Figure 6)

(A) HeLa cells, siRNA-depleted for the indicated proteins, were released from a double thymidine block in the presence of WEE1i or DMSO. DNA content was analyzed by FACS. **(B)** HeLa cells, siRNA-depleted for the indicated proteins, were synchronized by a double thymidine block and released in the presence of WEE1i or DMSO. Time-lapse microscopy was used to follow mitotic cell rounding, with pictures taken at 10-minute intervals. Mitotic index over the course of 22 hours is depicted for cells treated with DMSO (left graph) or WEE1i (right graph). For comparison purposes the "DMSO siControl" data is also displayed in the right graph. Corresponding mitotic entry data is plotted in Figure 6E.

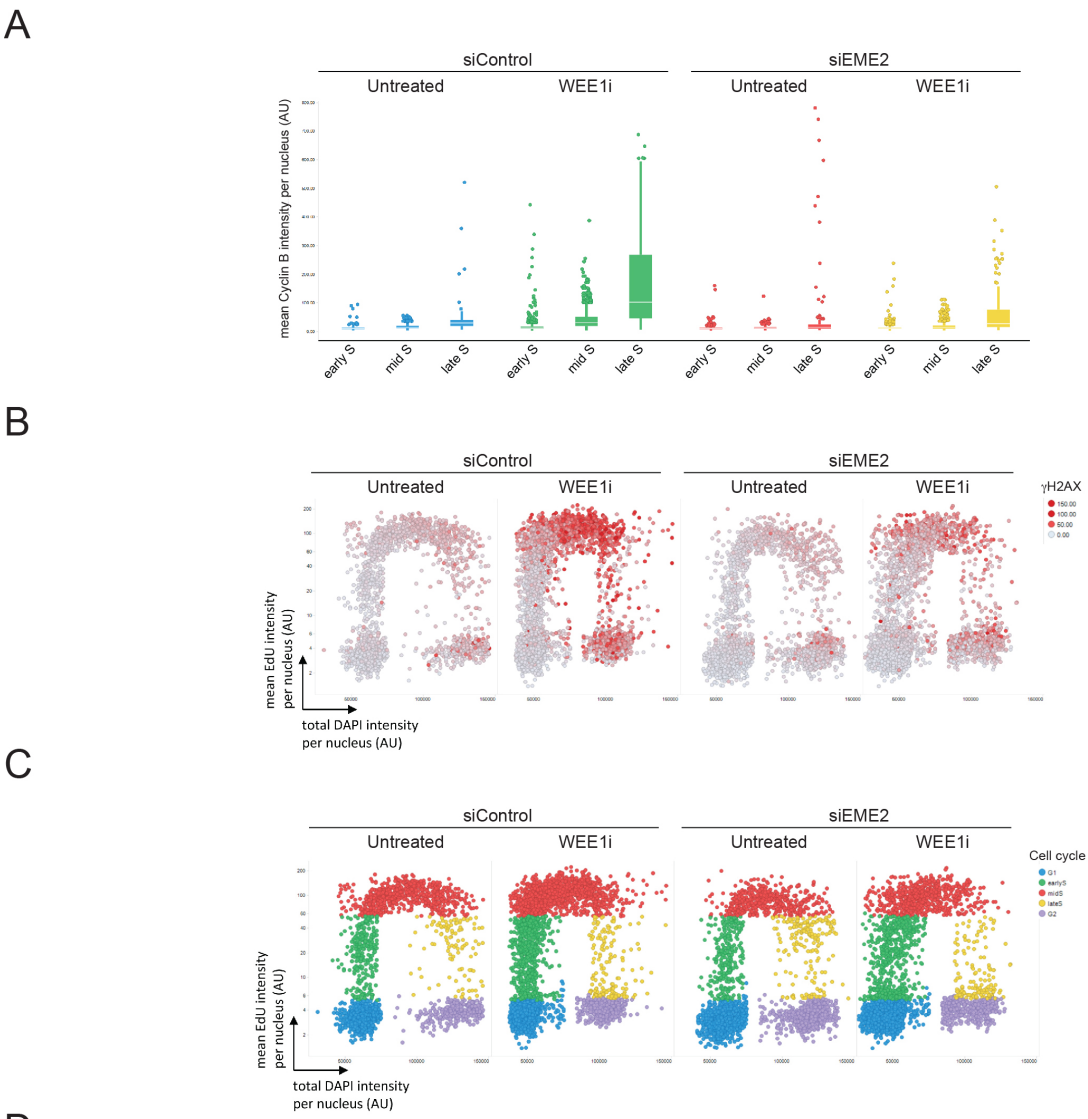

Figure S6. WEE1 inhibition causes premature entry into mitosis in asynchronous cells. (Related to Figure 6)

(A) Scatter plot of the QIBC data from Figure 6F, displaying mean Cyclin B intensities at different stages of S-phase. Box shows the median value. **(B)** QIBC data from **Figure 6F**. Scatter plots depict mean EdU intensities versus total nuclear DAPI intensities. Color-code: Mean γ-H2AX levels. **(C)**

QIBC data from **Figure 6F**. Scatter plots depict mean EdU intensities versus total nuclear DAPI intensities. Color code: G1, Blue ; early S, Green ; mid S, Red ; late S, Yellow; G2/M, Purple. **(D)** Representative images of the QIBC data from **Figure 6F**.

Figure S7

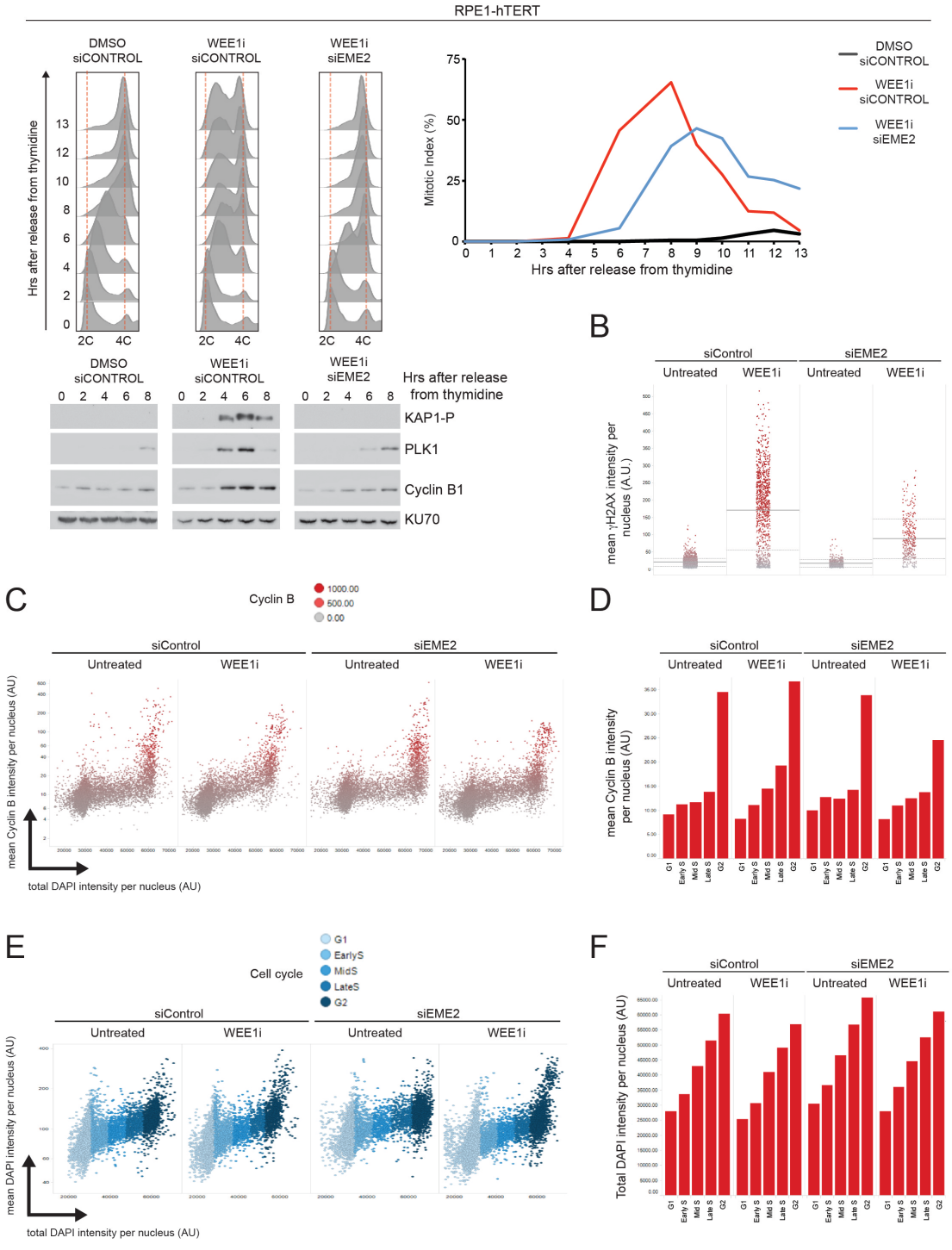

Figure S7. WEE1 inhibition causes DNA damage and EME2-dependent premature entry into M-phase in RPE1-hTERT cells (Related to Figure 7)

(A) RPE1-hTERT cells, siRNA-depleted for the indicated proteins, were synchronized by a single thymidine block and released in the presence of WEE1i (2.5 μM) or DMSO. DNA content was analyzed by FACS; pictures taken at 1-hour intervals to monitor mitotic index; Western blot analysis of soluble extracts from samples collected at 2-hour intervals is shown for the indicated proteins. Note: The population of cells in G1 that were not synchronized by thymidine at t=0 hr (approx. 20%) was gated out at all time points in order to facilitate visualization of progression through S-phase. **(B)**

Asynchronously proliferating RPE1-hTert cells were treated with siRNAs as indicated and exposed to WEE1i (2.5 μM) for 3h, stained for γ-H2AX and analyzed by quantitative image-based cytometry. Scatter plots depict mean γ-H2AX levels in the whole population. **(C)** Asynchronously proliferating RPE1-hTERT cells were treated as in **(B)**, stained for Cyclin B and DAPI, and analyzed by quantitative image-based cytometry. Scatter plots depict mean nuclear Cyclin B levels versus total nuclear DAPI intensities. Color-code: Mean Cyclin B levels. **(D)** The bar chart depicts mean nuclear Cyclin B levels from **(C)** in cell cycle staged population averages according to their DAPI profiles in **(E and F)**. **(E)** Cell cycle staging and gating of cells analyzed in **(C and D)** by quantification of DNA content (DAPI) using QIBC. **(F)** The bar chart depicts total DAPI intensity per nucleus from cells in **(C)**.

SUPPLEMENTAL MOVIE LEGENDS

Movie S1. Time-lapse recording of HeLa cells expressing Histone 2B-mCherry treated with WEE1i (Related to Figure 5)

(A) Cells were released from a double thymidine block and treated with DMSO. Pictures were taken every 10 minutes following release from the second thymidine block. Time post thymidine release is indicated. **(B)** Cells were released from a double thymidine block and treated with WEE1i (500 nM). Pictures were taken every 10 min following release from the second thymidine block. Time post thymidine release is indicated. **(C)** Cells transfected with siRNAs targeting EME2 were released from a double thymidine block and treated with WEE1i (500 nM). Pictures were taken every 10 min following release from the second thymidine block. Time post thymidine release is indicated.

Movie S2. Time-lapse recording of control HeLa cells treated with WEE1i (Related to Figure 6)

(A) Cells transfected with control siRNAs were released from a double thymidine block and treated with DMSO. Pictures were taken every 10 min following release from the second thymidine block. Time post thymidine release is indicated. **(B)** Cells transfected with control siRNAs were released from a double thymidine block and treated with WEE1i. Pictures were taken every 10 min following release from the second thymidine block. Time post thymidine release is indicated. **(C)** Cells transfected with siRNAs targeting EME2 were released from a double thymidine block and treated with WEE1i. Pictures were taken every 10 min following release from the second thymidine block. Time post thymidine release is indicated.

SUPPLEMENTAL EXPERIMENTAL PROCEDURES

Tissue culture and cell lines

RPE1-hTERT, HAP1 (Carette et al., 2011), HeLa FRT/TO and HeLa Kyoto cells were maintained in Dulbecco's Modified Eagle Media (DMEM), supplemented with 10% fetal bovine serum (FBS). FA-P cells were maintained in DMEM supplemented with 20% FBS. All cultures were grown at 37°C in a humidified atmosphere containing 5% or 10% CO_2.

HAP1 cells carrying CRISPR/Cas9-induced mutations in MUS81 (HAP1_MUS81_14843-02), EME1 (HAP1_EME1_07401-04) and EME2 (HAP1_EME2_01949-12) were purchased from Haplogen Genomics. HAP1 cell lines were initially haploid (~1n) but quickly stabilized their DNA content at a diploid (~2n) level, as assayed by FACS. All experiments were performed with ~2n HAP1 cells.

Stable HeLa FRT/TO cell lines modified with siRNA-resistant MUS81-WT-SF, MUS81-ND-SF (nuclease-dead, D307A), SLX4-WT-Venus-FLAG, SLX4-41A-Venus-FLAG, SLX4-35A-Venus-FLAG or SLX4-6A-Venus-FLAG, were induced with 1 mg/mL doxycycline 20-24 hours prior to harvesting. SF: StrepII-FLAG tag (Gloeckner et al., 2009); pcDNA5/FRT/TO-Venus-Flag-Gateway (1124) was a gift from Jonathon Pines (Addgene plasmid # 40999). *SLX4-41A* was prepared by gene synthesis (GeneArt, Thermo Fisher Scientific). *SLX4-35A and SLX4-6A* were prepared by swapping a restriction fragment (BstBI, EcoRI) between *SLX4-41A* and *SLX4-WT*

HeLa Kyoto cells stably expressing MUS81-FLAP (CLJM6) (Matos et al., 2011) or SLX4-FLAP (CLJM59) (this study) were generated using BAC recombineering (Poser et al., 2008).

Note 1: While analyzing MUS81 levels in the HAP1 KO cell lines we made an unexpected observation. Introduction of a frameshift mutation in Exon 2 eliminated the full-length MUS81 protein, as predicted. However, it did not alter the levels of a faster migrating protein that cross-reacted with anti-MUS81 antibodies ($MUS81_{short}$, ~50 kDa) (Figures 4F and S4F). In contrast, a frameshift mutation in Exon 3 led to elimination of both forms of MUS81 (data not shown). $MUS81_{short}$ is detected in a variety of additional cell lines, such as HeLa Kyoto, U2OS and RPE1-hTERT, and can be efficiently depleted by siRNAs targeting exon 14 of MUS81 (Figure S4A). Interestingly, a protein-coding splice variant of MUS81, that lacks Exon1 and most of Exon 2, has been predicted (Figure S4F). This variant would encode a version of MUS81 lacking the first 75 residues, which are required for association with SLX4 (Fekairi et al., 2009). Indeed, whereas $MUS81_{short}$ could be readily detected alongside

MUS81 in EME1 immunoprecipitates, SLX4 immunoprecipitates specifically lacked $MUS81_{short}$ (Figure 2D, S2A, S2C and data not shown). These observations raise the interesting possibility that in order to enable MUS81 to carry out SLX4-independent functions during mitosis, human cells evolved $MUS81_{short}$, which is unable to associate with SLX4.

Short-term and long-term cell survival assays

HAP1 cells of the indicated genotypes were seeded into Lab-Tek II.8-Wells chambers (Milian SA). Cells were treated with DMSO or 500 nM MK-1775 and followed by time-lapse microscopy at 5-minute intervals for 22 hours. Short term cell survival was calculated by determining the fraction of living cells to the total number of cells in the first (t = 2 h, set to 100% survival) and last (t = 22 h) frame of the movie and expressed as %. The shown numbers were averaged from 3 independent experiments.

Long-term survival of HAP1 cells was determined using a clonogenic assay. In brief, HAP1 cell lines were plated at a density of 1000 cells per well in six-well plates and were allowed to adhere overnight. Cells were then treated with MK-1775 at final concentrations from 50 nM to 500 nM, or DMSO as a control. The drug was removed after 6 hours, followed by two washes with PBS, and cells were incubated in fresh medium. After one week, cells were fixed and stained with crystal violet solution (1% formaldehyde, 0.05 % crystal violet, 1% methanol). Plates were air-dried and the number of colonies on each plate was counted.

Cell survival of FA-P cells was determined using a luciferase-based microtiter plate assay. In brief, FA-P cells were plated at a density of 1000 cells per well in opaque white 96-well plates (BD Biosciences, 353296) in triplicates and were allowed to adhere overnight. Cells were then treated with MK-1775 at final concentrations from 400 to 1200 nM, or DMSO as a control. The drug was removed after 6 hours, followed by two washes with PBS and cells were re-fed with growth medium (DMEM, supplemented with 20% FBS). Cell survival was determined five days later using the Cell Titer-Glo 2.0 reagent (Promega) on a CLARIOStar microplate reader (BMG Labtech) according to the manufacturer's instructions.

siRNA transfections and western blotting

For siRNA-mediated protein depletion, cells were plated to ~30% confluency, 10-12 hr prior to transfection. In all experiments, cells were transfected using Lipofectamine RNAiMAX (Invitrogen). ON-TARGETplus siRNAs and siMax siRNAs were purchased from Dharmacon and Eurofins, respectively. The sequences (5′ to 3′) are as follows:

MUS81: CAGCCCUGGUGGAUCGAUAUU (Wechsler et al., 2011)

EME2: GCGAGCCAGUGGCAAGAGA (Pepe and West, 2014)

SLX1: UGGACAGACCUGCUGGAGAUU (Munoz et al., 2009)

SLX4: (#1) AAACGUGAAUGAAGCAGAAUU; (#2) CGGCAUUUGAGUCUGCAGGUGUU; (Munoz et al., 2009; Wechsler et al., 2011)

On-TARGETplus non-targeting pool (Dhamacon) #D-001810-10-20

Non-specific control (Eurofins): UAAUGUAUUGGAACGCAUA

Two rounds of siRNA transfection were used for MUS81 depletion, ~24 and ~48 hours before the experiment.

The efficiency of protein depletion was monitored by western blotting 44-60 hr after transfection.

Synchronization and mitotic time courses

To obtain cell cycle stage-specific synchronization, sub-confluent cells were treated for 18 hr with thymidine (2 mM) or for 15 hr with nocodazole (150 ng/ml). To follow the progression of G1/S arrested cells into mitosis, cells were synchronized with a double thymidine block (15-16 hours) and released into pre-warmed medium containing appropriate amounts of the following kinase inhibitors (or equivalent volumes of the appropriate solvents): WEE1 inhibition in HeLa Kyoto –400-500 nM MK-1775; 100-500 nM MK-1775 in HAP1 cells; 2.5 μM MK-1775 was used in RPE1-hTERT cells; 400-1200 nM MK-1775 was used in FA-P cells. MK-1775 was purchased from Selleck Chemicals, batches S152501, S152503 and S152504. PLK1 inhibition - 200 nM BI2536 (Selleck Chemicals); CDK1 inhibition – 9 μM RO-3306 (Sigma). siRNA treatments were done 45-48 hours prior to release from the second thymidine block.

The mitotic index was calculated by determining the fraction of rounded-up cells to the total number of cells and expressed as %. Images were acquired every hour using a Leica DM IL microscope with an Olympus C-7070 Wide Zoom camera. > 200 cells were inspected for each time point.

Time-lapse microscopy

HeLa Kyoto cells were seeded into Lab-Tek II.8-Wells chambers (Milian SA), siRNA-depleted for the indicated proteins, and synchronized by a double thymidine block (15-16 hours). Cells were released into pre-warmed Leibovitz's L-15 medium without Phenol Red (Gibco) supplemented with 10% fetal bovine serum (FBS), which contained MK-1775 (WEE1i) or the corresponding amount of DMSO. The chambers were then transferred to a Zeiss 200M microscope outfitted with a Zeiss LifeCell station system controlled by Metamorph 7.7.11 software (Molecular Devices) or an Olympus IX 81 microscope with an Olympus MM system controlled by Metamorph 7.7.7 software in an incubator box set to 37°C. Per condition, 3 positions were marked and imaged automatically every 10 min for 20-22 hrs (starting 1.5 to 2 hours after release from the second thymidine block) using a 20x 0.8NA Plan Apochromat or a 20x 0.75NA UPlanSApo air objective and an ORCA-flash 4.0 V2 camera (Hamatsu). The progression of mitosis was followed by observing cell (DIC) and chromatin (H2B-mCherry fluorescence) morphology changes during the time course. Mitotic entry was defined as the first frame in which the cell had fully rounded up. Mitotic index was calculated as the fraction of rounded cells at a given time to the total number of rounded cells in the movie. Only living cells were counted.

Metaphase plate formation and nuclear division were quantified in HeLa Kyoto cells stably expressing histone H2B-mCherry (Schmitz et al., 2010) (kindly provided by Daniel Gerlich, IMBA Vienna), and expressed as % of all rounded up cells or % of all rounded up cells that reattached during the video, respectively. Time-lapse images were acquired on an Olympus IX71 microscope outfitted with a DeltaVision Measure system controlled by Softworx 4.1.0 software (Applied Precision). Calculations and statistics were performed using Microsoft Excel and Graph Pad Prism.

Immunofluorescence Microscopy

HeLa Kyoto cells were grown on glass coverslips (ThermoScientific) added to the culture dishes, treated as indicated and then permeabilized with 0.3% Triton-X100 for 10 min on ice, followed by 20 min fixation with 4% paraformaldehyde on ice and 1 min incubation with ice cold methanol. Cells were blocked for 1 h in 3% BSA + 0.05 % Tween 20 and incubated overnight with primary antibodies in BSA-Tween. The primary antibodies used were: rabbit anti-TOPBP1 (1:2000 or 1:1000, Abcam), mouse anti-MUS81 (1:1000, MTA30 2G10), rabbit anti-GFP (1:5000), mouse anti-GFP (1:1000, Roche), mouse anti-γ-H2AX (1:5000, Abcam). Secondary antibodies conjugated to Alexa555 (1:1000, Chemicon) and Alexa488 (1:1000, Chemicon) were used for detection. DNA was stained with DAPI and coverslips were mounted on microscope slides (Thermo Scientific) using ProLong® Gold Antifade Reagent (Life Technologies).

Images were acquired using a Leica DM 6000B microscope using a HCX PL Fluotar x63, oil objective lens, and captured using an ORCA C4742-95-12ER camera (Hamamatsu) controlled by Openlab 5.0.2 software (Improvision). Images were processed using Adobe Photoshop CS6 extended.

Mean foci number was calculated by averaging the number of fluorescent foci in 2-3 independent experiments. Colocalization (expressed in %) was calculated by determining the fraction of foci that displayed co-staining to the total number of detected foci. ≥ 30 cells were inspected per condition and experiment. Calculations and statistics were performed using Graph Pad Prism or Microsoft Excel.

Quantitative Image-Based Cytometry (QIBC)

Automated multichannel wide-field microscopy for quantitative image-based cytometry (QIBC, Figures 3H and I, 6F-I, S3B and C, S6A-D and S7B-F) was performed as described (Altmeyer et al., 2013; Toledo et al., 2013) on an Olympus ScanR Screening System equipped with an inverted motorized Olympus IX83 microscope, a motorized stage, IR-laser hardware autofocus, a fast emission filter wheel with single band emission filters, and a 12bit digital monochrome CMOS camera with sensor chip FL-400 (2048 x 2048 pixels of size 6.5 x 6.5 µm). Images were acquired either with a 4x (NA 0.16) or 10x (NA 0.4) objective under non-saturating conditions. All images were analyzed by the inbuilt Olympus ScanR Image Analysis Software Version 2.5.1, a dynamic background correction was applied, and nuclei segmentation was performed using an integrated intensity-based object detection module. Pulsed 5-ethynyl-2'-desoxyuridine (EdU, Thermo Fisher) incorporation, total DAPI, mean intensities of Cyclin B (BD Transduction Laboratories C23420, 1:500), chromatin-bound RPA70 (Abcam ab79398, 1:500) and γH2AX (Biolegend 613401, 1:1000; Cell Signaling 9718, 1:500) were analysed. Color-coded scatter plots of asynchronous HeLa and RPE1-hTERT cell populations were generated with Spotfire data visualization software (TIBCO).

Analysis of metaphase chromosomes

Cells were treated with 0.2 µg/ml colcemid 40-60 min prior to collection by mitotic shake-off, washed in PBS and swollen in 5 ml of 75 mM KCl for 15-30 min at 37°C. Ice-cold methanol/acetic acid (3:1 ml) was added on top of the swelling buffer and the cells were centrifuged for 5 min at 800 rpm at RT. The two-layered solution was removed and the cells were fixed in 5 ml of ice-cold methanol/acetic acid (15 min on ice). Metaphase cells were then spread on microscope slides (Thermo Scientific) and washed with 2ml ice-cold methanol/acetic acid. After O/N air drying, surface spreads were stained with 7% Giemsa for 7-10 minutes.

After washing with 50 ml water and air-drying overnight, coverslips were mounted on the slides using DPX mounting medium (Merck Millipore) or Permount (Fisher Scientific).

Images were acquired using a Leica DM 6000B microscope using a HCX PL Fluotar x63, oil objective lens, and captured using an ORCA C4742-95-12ER camera (Hamamatsu) controlled by Openlab 5.0.2 software (Improvision) or using an Olympus BX50 microscope using an UPlanApo 100x oil objective lens, and captured using an Sensicam XVGA (PCO) camera controlled by Live Acquisition 2.5.0.26 software (FEI Life Sciences).

Pulsed-field gel electrophoresis

PFGE was performed as previously described (Hanada et al., 2007; Pepe and West, 2014). Briefly, $5x10^5$ Hela Kyoto cells were used to make low melting point agarose plugs using CHEF Mapper® XA system plug molds (Bio-Rad). Cells were centrifuged, resuspended in 50 µl of washing buffer (10 mM Tris-HCl pH 8.0, 100 mM EDTA) and mixed with 50 µl 1% (w/v) low melting point agarose in water. After polymerization at 4°C, plugs were incubated with lysis buffer (10 mM Tris-HCl pH 8.0, 100 mM EDTA, 1% (w/v) sodium lauryl sarcosine, 0.2% (w/v) sodium deoxycholate and 1 mg/ml proteinase K) at 37°C for 48 hours. Plugs were washed 2x in washing buffer and incubated overnight with RNase (10 mM Tris-HCl pH 8.0, 10 mM EDTA, 1 mg/ml RNase A). Plugs were then washed in 10 mM Tris-HCl pH 8.0 and 100 mM EDTA, and loaded onto a 1% (w/v) agarose gel in 0.5% (v/v) TBE. Gels were run for 23 hr at 13°C in a Gene Navigator PFGE apparatus (Amersham Biosciences) using the following parameters: voltage 180–120 V log; angle from 1201 to 1101 linear; interval 30 s to 5 s log. Gels were stained with 1.25 µg/ml ethidium bromide in 0.5% (v/v) TBE for 1 hr, washed in TBE and visualized using a GelDoc XR+ imager (Bio-Rad). Band quantifications were performed using ImageLab software.

FACS analysis of DNA content

Hela Kyoto cells were treated with trypsin, washed with PBS and fixed in ice-cold 70% ethanol overnight at 4°C. Prior to cytometric analysis, cells were washed with PBS and incubated with 50 µL of 100 µg/mL RNase A (Qiagen) and 200 µL of 50 µg/mL propidium iodide (Sigma).

Cellular DNA content was determined using a FACSCalibur flow cytometer (BD Biosciences) and FACS data were analyzed using FlowJo 10.1 software.

Protein extraction, immunoprecipitations and western blotting

Cells were washed in PBS, lysed in 500 µL LAP buffer, as previously described (Matos et al., 2011), and insoluble material was removed by centrifugation. Cleared lysates were normalized for total protein content (2-5 mg) and incubated with 15 µL of GFP-Trap matrix (Chromotek) for 90 min at 4°C (rotating wheel), followed by extensive washing with LAP buffer.

Whole-cell lysates or immunoprecipitates were subjected to NuPAGE gel electrophoresis (NuPAGE 3-8% Tris-Acetate; NuPAGE 7% Tris-Acetate or NuPAGE BOLT 4-12% Bis-Tris, Invitrogen) and blotted on PVDF membranes (GE Healthcare). Proteins were detected using mouse anti-MUS81 (Santa Cruz MTA30 2G10), mouse anti-GFP (Roche), mouse anti-EME1 (Santa Cruz MTA31 7H2), mouse anti-PLK1 (Santa Cruz sc-17783), mouse anti-γ-H2AX (1:5000, Abcam), rabbit anti-SLX4 (APE11, (Wyatt et al., 2013)), rabbit anti-SLX4 (A302-270A, Bethyl), rabbit anti-EME2 (APE13 (Pepe and West, 2014)), rabbit anti-cyclin E (Santa Cruz), Rabbit anti-H3-P (Abcam), rabbit anti-γ-H2AX (Abcam), rabbit anti-KAP1 (Abcam), apoptosis-detection cocktail (Abcam ab136812), rabbit anti-CYK4-P-S157 (a gift from Mark Petronczki and Tohru Takaki), mouse anti-Cyclin B (BD), rabbit anti-Cdc2-Y15-P (Cell Signaling Technology), mouse anti-CDC27 (BD), mouse-anti CHK1 (Santa Cruz sc-8408), rabbit-anti CHK1-S345-P (Cell Signaling), rabbit-anti RPA32 (A300-244 A, Bethyl Laboratories), rabbit-anti RPA32-S33-P (A300-246A, Bethyl Laboratories).

Nuclease assays

For nuclease assays, MUS81-FLAP and SLX4-FLAP were immuno-affinity purified using GFP-Trap (Chromotek) beads and washed extensively. The beads (approx. volume 10 µl) were then mixed with 10 µl cleavage buffer (50 mM Tris-HCl pH 7.5, 3 mM $MgCl_2$, 10 ng/µl poly[dI-dC]) and approximately 1 nM 5'-^{32}P-end-labeled synthetic Holliday junction (X26), 1 nM 5'-^{32}P-end-labeled synthetic replication fork, or 15 ng 5'-^{Cy3}-end-labeled synthetic replication fork (Ip et al., 2008). After incubation at 37°C with gentle rotation (10-15 min for RFs; 45 min for HJs), reactions were stopped by addition of 3 µl of 10 mg/ml proteinase K and 2% SDS, followed by incubation for 45 min at 37°C. Loading dye (4 µl) was then added and the labeled products were separated by 10% native PAGE and analyzed by phosphorimaging or fluorescence scanning using a Typhoon scanner. Band intensities were determined using ImageQuant software (GE Healthcare). Resolution activity (% of cleavage) was calculated by determining the fraction of nicked duplex DNA product relative to the sum of the intact substrate and resolution product.

SUPPLEMENTAL REFERENCES

Altmeyer, M., Toledo, L., Gudjonsson, T., Grofte, M., Rask, M.B., Lukas, C., Akimov, V., Blagoev, B., Bartek, J., and Lukas, J. (2013). The chromatin scaffold protein SAFB1 renders chromatin permissive for DNA damage signaling. Mol Cell *52*, 206-220.

Carette, J.E., Raaben, M., Wong, A.C., Herbert, A.S., Obernosterer, G., Mulherkar, N., Kuehne, A.I., Kranzusch, P.J., Griffin, A.M., Ruthel, G.*, et al.* (2011). Ebola virus entry requires the cholesterol transporter Niemann-Pick C1. Nature *477*, 340-343.

Fekairi, S., Scaglione, S., Chahwan, C., Taylor, E.R., Tissier, A., Coulon, S., Dong, M.Q., Ruse, C., Yates, J.R., 3rd, Russell, P.*, et al.* (2009). Human SLX4 is a Holliday junction resolvase subunit that binds multiple DNA repair/recombination endonucleases. Cell *138*, 78-89.

Gloeckner, C.J., Boldt, K., Schumacher, A., and Ueffing, M. (2009). Tandem affinity purification of protein complexes from mammalian cells by the Strep/FLAG (SF)-TAP tag. Methods in molecular biology *564*, 359-372.

Hanada, K., Budzowska, M., Davies, S.L., van Drunen, E., Onizawa, H., Beverloo, H.B., Maas, A., Essers, J., Hickson, I.D., and Kanaar, R. (2007). The structure-specific endonuclease Mus81 contributes to replication restart by generating double-strand DNA breaks. Nature structural & molecular biology *14*, 1096-1104.

Ip, S.C.Y., Rass, U., Blanco, M.G., Flynn, H.R., Skehel, J.M., and West, S.C. (2008). Identification of Holliday junction resolvases from humans and yeast. Nature *456*, 357-361.

Matos, J., Blanco, M.G., Maslen, S., Skehel, J.M., and West, S.C. (2011). Regulatory control of the resolution of DNA recombination intermediates during meiosis and mitosis. Cell *147*, 158-172.

Munoz, I.M., Hain, K., Declais, A.C., Gardiner, M., Toh, G.W., Sanchez-Pulido, L., Heuckmann, J.M., Toth, R., Macartney, T., Eppink, B.*, et al.* (2009). Coordination of structure-specific nucleases by human SLX4/BTBD12 is required for DNA repair. Molecular Cell *35*, 116-127.
Pepe, A., and West, S.C. (2014). MUS81-EME2 Promotes Replication Fork Restart. Cell reports *7*, 1048-1055.
Poser, I., Sarov, M., Hutchins, J.R., Heriche, J.K., Toyoda, Y., Pozniakovsky, A., Weigl, D., Nitzsche, A., Hegemann, B., Bird, A.W.*, et al.* (2008). BAC TransgeneOmics: a high-throughput method for exploration of protein function in mammals. Nature methods *5*, 409-415.
Schmitz, M.H., Held, M., Janssens, V., Hutchins, J.R., Hudecz, O., Ivanova, E., Goris, J., Trinkle-Mulcahy, L., Lamond, A.I., Poser, I.*, et al.* (2010). Live-cell imaging RNAi screen identifies PP2A-B55alpha and importin-beta1 as key mitotic exit regulators in human cells. Nature cell biology *12*, 886-893.
Toledo, L.I., Altmeyer, M., Rask, M.B., Lukas, C., Larsen, D.H., Povlsen, L.K., Bekker-Jensen, S., Mailand, N., Bartek, J., and Lukas, J. (2013). ATR prohibits replication catastrophe by preventing global exhaustion of RPA. Cell *155*, 1088-1103.
Wechsler, T., Newman, S., and West, S.C. (2011). Aberrant chromosome morphology in human cells defective for Holliday junction resolution. Nature *471*, 642-646.
Wyatt, H.D., Sarbajna, S., Matos, J., and West, S.C. (2013). Coordinated actions of SLX1-SLX4 and MUS81-EME1 for Holliday junction resolution in human cells. Mol Cell *52*, 234-247.